iScience

CellPress
OPEN ACCESS

Article

The gut microbiota of people with asthma influences lung inflammation in gnotobiotic mice

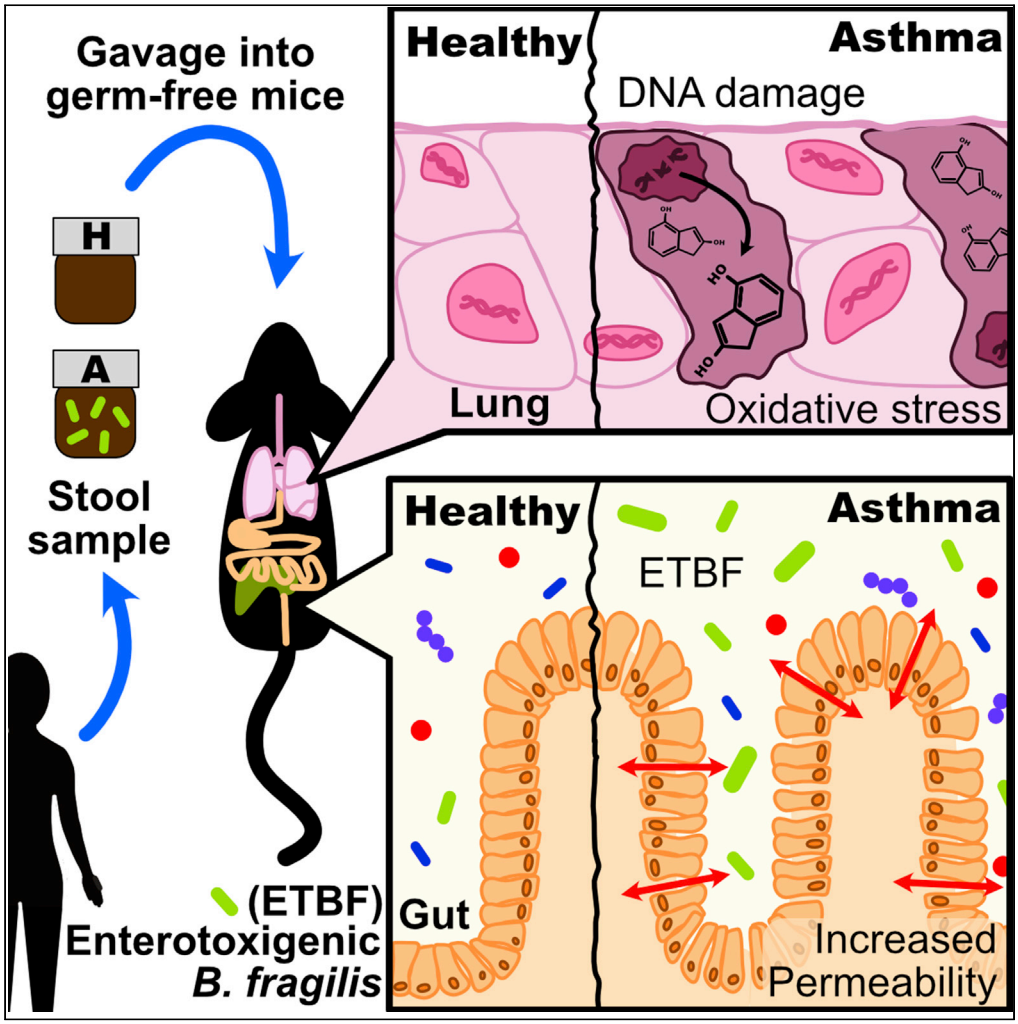

Naomi G. Wilson, Ariel Hernandez-Leyva, Anne L. Rosen, ..., Leonard B. Bacharier, S. Joshua Swamidass, Andrew L. Kau

akau@wustl.edu

Highlights

Gut microbiota (GM) of patients with asthma differs from that of healthy controls

GM from humans with asthma alters features of AAI in gnotobiotic mice

ETBF increases gut barrier permeability and lung oxidative stress in a model of AAI

ETBF is more prevalent in patients with asthma compared to healthy individuals

Wilson et al., iScience 26, 105991
February 17, 2023
https://doi.org/10.1016/j.isci.2023.105991

iScience

CellPress
OPEN ACCESS

Article

The gut microbiota of people with asthma influences lung inflammation in gnotobiotic mice

Naomi G. Wilson,[1,4] Ariel Hernandez-Leyva,[1,4] Anne L. Rosen,[1] Natalia Jaeger,[1] Ryan T. McDonough,[1] Jesus Santiago-Borges,[1] Michael A. Lint,[1] Thomas R. Rosen,[1] Christopher P. Tomera,[1] Leonard B. Bacharier,[2] S. Joshua Swamidass,[3] and Andrew L. Kau[1,5,*]

SUMMARY

The gut microbiota in early childhood is linked to asthma risk, but may continue to affect older patients with asthma. Here, we profile the gut microbiota of 38 children (19 asthma, median age 8) and 57 adults (17 asthma, median age 28) by 16S rRNA sequencing and find individuals with asthma harbored compositional differences from healthy controls in both adults and children. We develop a model to aid the design of mechanistic experiments in gnotobiotic mice and show enterotoxigenic *Bacteroides fragilis* (ETBF) is more prevalent in the gut microbiota of patients with asthma compared to healthy controls. In mice, ETBF, modulated by community context, can increase oxidative stress in the lungs during allergic airway inflammation (AAI). Our results provide evidence that ETBF affects the phenotype of airway inflammation in a subset of patients with asthma which suggests that therapies targeting the gut microbiota may be helpful tools for asthma control.

INTRODUCTION

Asthma is a common respiratory disease characterized by airway inflammation triggered by an allergic response to environmental antigens. Although asthma is predominately associated with T helper (Th)-2 inflammation associated with high levels of cytokines IL-4, IL-5, and IL-13, detailed characterization from clinical studies has revealed substantial heterogeneity in the immunopathology of this disease, referred to as an asthma endotype.[1] The majority of children tend to have a Th2-dominant endotype and often experience virus-induced exacerbations. In contrast, a significant fraction of adults have a non-Th2 driven endotype and experience a wider spectrum of immunopathologies.[2] For example, Th17-associated inflammation is more common in adults and is associated with corticosteroid resistance and increased frequency of exacerbations.[3] Furthermore, greater intracellular oxidative stress increases inflammation and hyperreactivity in the airways of patients with asthma[4] and has been associated with IL-17A mediated inflammation in mouse models.[5] Although disease heterogeneity plays an important role in the prognosis and treatment of asthma, the specific factors that drive the endotype of asthma are not well understood.

A potential source of disease variability in the lung lies in the diverse immunologic and metabolic activities of the gut microbiota. Gut microbes have been implicated in the pathology of a range of lung diseases including chronic obstructive pulmonary disease,[6] fungal[7] and bacterial pneumonia,[8,9] and, notably, asthma.[10] One mechanism by which this phenomenon, termed the "gut-lung" axis,[11] affects asthma is through the synthesis of bioactive metabolites. For example, microbe-derived molecules like short-chain fatty acids[10,12] and 12,13-diHOME[13,14] are thought to permanently alter the immune system during infancy. Other metabolites produced by the gut microbiota have also been shown to influence oxidative stress in distal tissues including the brain and kidneys later in life.[15,16]

Metagenomic surveys have revealed a "critical window"[17] where microbiome and immune co-development[18] during the first year of life has an exaggerated effect on the development of asthma later in life.[10,19–21] In addition, gnotobiotic animal studies have shown that asthma-associated microbes from early childhood can modulate susceptibility to experimental models of AAI.[10] However, it remains unclear whether the mechanisms influencing the development of asthma in infants continue to affect the disease in older children and adults, or whether functions of the gut microbiota modulate the characteristics of asthma after it has been established.

[1]Division of Allergy and Immunology, Department of Medicine and Center for Women's Infectious Disease Research, Washington University School of Medicine, St. Louis, MO 63110, USA

[2]Division of Allergy, Immunology and Pulmonary Medicine, Department of Pediatrics, Monroe Carell Jr Children's Hospital at Vanderbilt University Medical Center, Nashville, TN 37232, USA

[3]Department of Pathology and Immunology, Washington University School of Medicine, St. Louis, MO 63110, USA

[4]These authors contributed equally

[5]Lead contact

*Correspondence: akau@wustl.edu

https://doi.org/10.1016/j.isci.2023.105991

Among older children and adults that are beyond the critical window, individuals with asthma harbor differences in microbial diversity and composition[22–25] compared to healthy controls, emphasizing the need to further investigate the influence the microbiota might have on asthma throughout life.

Few studies have been devoted to identifying and defining the effects of the gut microbiota on lung inflammation in older individuals with asthma. One of these studies has demonstrated that the gut commensal, *Akkermansia muciniphila*, which is reduced in individuals with obesity-associated asthma, can mitigate AAI in mice.[25] In contrast, a study of AAI severity in gnotobiotic mice colonized with gut microbiota from school-aged children did not find a difference in markers of allergy between mice colonized with microbiota from healthy children and children with asthma.[26] Given these variable results, there remains a need to assess the effect of the gut microbiota on established asthma and to find testable mechanisms for human clinical studies.

In this study, our goal was to analyze the fecal microbiota from a clinical study of healthy and asthmatic subjects from which we could select representative human samples to thoroughly characterize in a gnotobiotic mouse model of AAI. Follow up experiments would then test the prevalence of the discovered immune phenotypes in additional fecal microbiota donors. We hypothesized that there would be effector gut microbes, more prevalent in people with asthma, that could promote airway inflammation in mice. Our results show that although typical markers of allergy were not affected by the gut microbiota, asthma-associated microbiomes were more likely to harbor enterotoxigenic *Bacteroides fragilis* (ETBF) which was associated with gut barrier dysfunction, as well as oxidative stress in the lungs of gnotobiotic mice.

Results

The composition of the gut microbiota differs between individuals with and without asthma

To investigate if asthma is associated with distinct gut microbial signatures outside of early childhood, we recruited 17 adults and 19 school-aged children with physician-diagnosed, moderate-to-severe atopic asthma with 40 adult and 19 school-aged healthy controls into the previously described Microbiome and Asthma Research Study[27] (MARS; see demographic summary in Table S1A and S1B and Figure S1A; see also STAR Methods). The adult cohort was 18–40 year-olds with a median age of 28 years (SD 6.2 years) and the pediatric cohort was 6–10 yearsold with a median age of 8 years (SD 1.6 years). We performed V4-16S rRNA amplicon sequencing of participant stool samples obtained at the patient's baseline and identified amplicon sequence variants (ASVs) using DADA2[28] (Figure S1B). There was a slight increase in alpha diversity in subjects as measured by Simpson's metric within individuals with asthma compared with healthy controls ($p = 0.035$), even after accounting for differences between age group ($p = 0.030$) and read depth ($p = 0.063$, Figure 1A). The significance of this trend is unclear however, as the same was not true for other metrics of alpha diversity which were more susceptible to read depth (Figure S1C). To determine how demographic features affected community composition we performed a PERMANOVA on Bray-Curtis dissimilarity distances (Figures 1B and S1D) between fecal microbiomes. First, we analyzed demographic factors reported to influence microbiome composition as independent terms using a sequential PERMANOVA and found that asthma status ($p = 0.00009$; $R^2 = 0.025$), age ($p = 0.00001$; $R^2 = 0.032$), and race ($p = 0.001$; $R^2 = 0.02$) significantly contributed to the variation in subject gut microbiota composition, but adiposity ($p = 0.3$; $R2 = 0.03$), sex ($p = 0.4$; $R2 = 0.009$), smoking history ($p = 0.4$; $R2 = 0.009$), and antibiotic exposure within the past year ($p = 0.7$; $R2 = 0.008$) did not (Table S2). We then ran another sequential PERMANOVA that included interaction terms between all the factors that had a p value of less than 0.05 in the first PERMANOVA and found that asthma status ($p = 0.02$; $R^2 = 0.015$), age ($p = 0.0017$; $R^2 = 0.019$), and race ($p = 0.0041$; $R^2 = 0.018$) remain contributors to the variation in beta diversity, even when accounting for sequencing batch effect and interaction terms (Figure 1C). Although age is an important factor in determining asthma phenotype, we did not find the interaction of age and asthma to be significant. Guided by the PERMANOVA results, we performed differential abundance analysis and identified alterations in taxa corresponding to disease status (11 ASVs), age (13 ASVs), and race (18 ASVs; see Table S3) after accounting for sequencing batch effect. Taxa differentially abundant between healthy and asthmatic individuals included several that have been previously reported to discriminate between healthy and atopic individuals including *Prevotella copri* (ASV8, ASV50)[29,30] and *Ruminococcus bromii*[31] (ASV119; Figure 1D).

Germ-free mice humanized with fecal microbiota from an adult with asthma showed an increase in lung oxidative stress and Th17 responses

We next sought to test whether the asthmatic gut microbiota could affect pulmonary inflammation in a mouse model of AAI. To explore this question, we selected a pair ("dyad") of human fecal microbiota samples from a

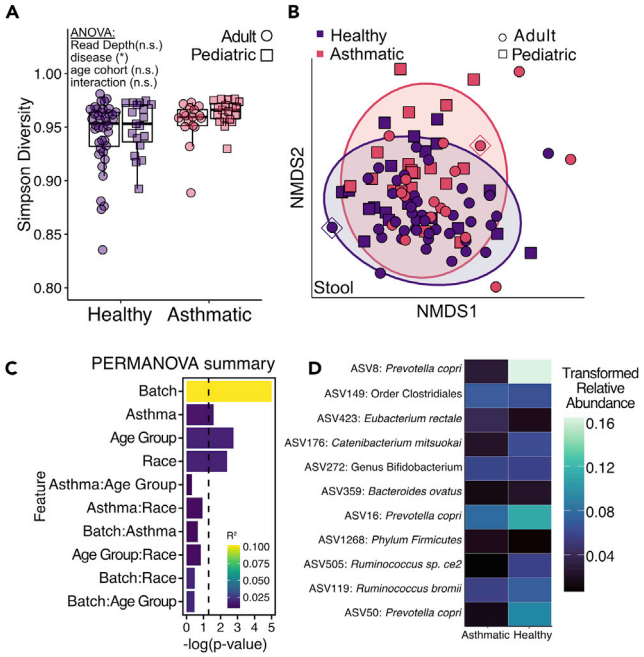

Figure 1. V4-16S rRNA profiling of stool from MARS cohort identifies gut microbiome differences in patients with asthma

(A) Simpson alpha diversity based on ASVs in stool samples from the MARS Cohort. Read depth was included as a variable to control for differences in library size.

(B) Non-metric multidimensional scaling (NMDS) on Bray-Curtis dissimilarity of MARS gut microbiomes. Ellipses represent 95% confidence intervals; diamonds indicate donor dyad (MARS0022/MARS0043).

(C) Bar plot summarizing results of PERMANOVA analysis on the beta diversity in (B). We also tested the homogeneity of the variance using PERMDISP2 and found no detectable difference in dispersion associated with age group or asthma status. Color represents R^2 value and the length of the bar represents-log(p value). Dashed line indicates a p value threshold of 0.05.

(D) Heatmap of average relative abundances of differentially abundant taxa identified between patients with asthma and healthy controls using DESEQ2. Average relative abundances have been rescaled using the arcsine-square-root transformation.

See also Figure S1.

healthy and asthmatic subject to "humanize" gnotobiotic mice by oral gavage. We initially selected an unrelated healthy-asthma dyad where the individuals were demographically similar (Subjects0022 and 0043; matched for age, sex, BMI, race, and smoking history, see Table S1C). We constructed a Naive Bayes Classifier (NBC) to generate several metrics that would help us evaluate the suitability of the selected dyad for characterization in a gnotobiotic animal model (see STAR Methods for additional details). First, to quantify how similar each sample was to its respective cohort, we calculated a Sample Score that ranged from 0 (typical of healthy) to 1 (typical of asthma) and found that both candidate donor microbiomes were typical of their respective disease cohorts (Figure 2A). Second, we visualized samples by Feature Score (Figures 2B and S2A–S2C, see STAR Methods) to confirm our selected samples cluster with their respective cohorts. Third, to evaluate the testable microbial relationships in the selected dyad relative to all other possible selections, we counted the number of ASVs, for all possible dyads agnostic to host demographics, whose relative abundance was consistent with the NBC's learned differences between the asthma and healthy cohorts. We defined this metric as a Pairwise Feature Score (PFS) which is greater than zero for every taxon in a dyad whose relative abundances are concordant with our model's predictions (see STAR Methods). We compared the number of "model concordant taxa" (PFS>0) between all possible dyads (Figures 2C and S2D) and found that our selected dyad contained a greater than average proportion of model concordant taxa. This indicates that the number of testable microbial comparisons mirroring the relationship between the asthma and healthy cohorts within our selected dyad is typical among all dyads. Together, these results support the idea that the demographically well-matched MARS0022-0043 dyad is characteristic of the microbial differences between cohorts and showcases a new tool for characterizing microbiome dyads.

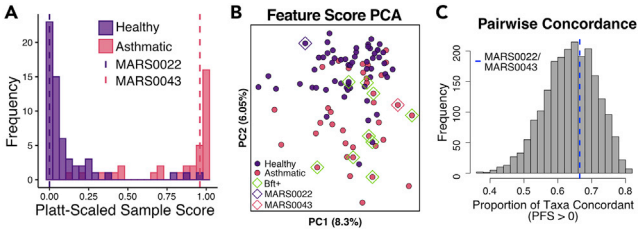

Figure 2. Selected donors capture discriminatory microbial relationships

(A) Histogram of Platt-scaled MARS NBC Sample Scores. A score of 0 is consistent with a "healthy appearing" sample and a score of 1 is consistent with an "asthma appearing" sample. Vertical dashed lines denote the sample scores for MARS0022 (purple) and MARS0043 (pink).

(B) PCA of NBC Feature Scores, calculated as the log likelihood that the relative abundance for a given taxon would occur in the healthy or asthma cohorts. MARS0022 (purple diamond) and MARS0043 (pink diamond) are the donor samples used in subsequent experiments in gnotobiotic mice. Green diamonds denote *bft* positive samples.

(C) Histogram of the proportion of pairwise concordant taxa across all possible healthy-asthma donor dyads. Vertical dashed line denotes the MARS0022 and MARS0043 dyad.

See also Figures S2, S8, and STAR Methods.

Mice humanized with the "healthy" (originating from MARS0022) or "asthmatic" (MARS0043) fecal microbiota underwent ovalbumin sensitization and challenge (OSC) or were sacrificed after 4 weeks without OSC, resulting in four groups of mice we will denote as follows: HO, mice colonized with a healthy microbiota undergoing OSC; AO, mice colonized with the asthmatic microbiota undergoing OSC; HN, mice colonized with a healthy microbiota that remained naive; AN, mice colonized with an asthmatic microbiota that remained naive (Figure 3A).

We performed V4-16S rRNA profiling of humanized gnotobiotic mice to better understand how gut microbial community ecology influences immune responses in the lung. This analysis affirmed that the gut microbial communities present in the gnotobiotic mice strongly resembled the human donors from which they had originated (Figures S3A and S3B). Although human fecal transplantation into gnotobiotic mice can result in some reconfigurations of the original community,[32] our analysis showed that many pairwise concordant taxa identified by our NBC colonized AO and HO gnotobiotic mice. These taxa included *Bacteroides uniformis*, *B. fragilis*, and Erysipelotrichaceae (*Longicatena caecimuris*), of which the latter two have been previously implicated in asthma pathogenesis[33–35] (Figure S3C).

To demonstrate that we successfully induced AAI in these mice, we performed bulk RNA-Seq on whole lungs and measured Th2 cytokines, *Il4*, *Il5* and *Il13* as well as serum anti-ovalbumin IgE. Although the degree of sensitization to ovalbumin and expression of Th2-related cytokines (*Il4*, *Il5*, or *Il13*) were markedly different between naive germ-free mice and both OSC treated groups, consistent with successful induction of AAI, we found no difference between AO and HO mice (Figures S4A and S4B). As expected, humanized mice undergoing OSC had transcriptome profiles that were distinct from naive humanized mice, reflecting upregulation of genes and pathways related to Type 2 and eosinophilic inflammation and demonstrating that we successfully induced AAI in HO and AO mice (Figures S4C–S4E, Tables S4, and S5).

We next evaluated the effect of the gut microbiota on overall lung transcriptome profiles. In naive mice, the gut microbiota appeared to have little or no effect on the overall transcriptome profiles because the difference between HN and AN mice was negligible (Figure 3B). In contrast, mice undergoing OSC colonized with different microbiota had distinct lung transcriptome profiles (see HO vs. AO mice in Figure 3B), suggesting the gut microbiota may be important in the context of AAI. Notably, expected allergy-related genes (*Il4*, *Il5*,*Il13*) and pathways (Type 2 immune response, hyperreactivity, eosinophil, and neutrophil pathways) that were upregulated by the induction of AAI were not differentially expressed between HO and AO mice (Figures S4A–S4C). These data suggest that Th2-related responses do not make up the transcriptomic differences between HO and AO mice.

Differentially abundant pathways between HO and AO mice included several involved in DNA repair and recombination (Figures 3C, S4F–S4G, Tables S4 and S5). We also saw enrichment of a pathway associated with the breakdown of hydrogen peroxide (GO:0042744) in HO compared to AO mice (Figures 3C and 3D). Many of the genes in this pathway have been implicated in protective responses to oxidative stress. These

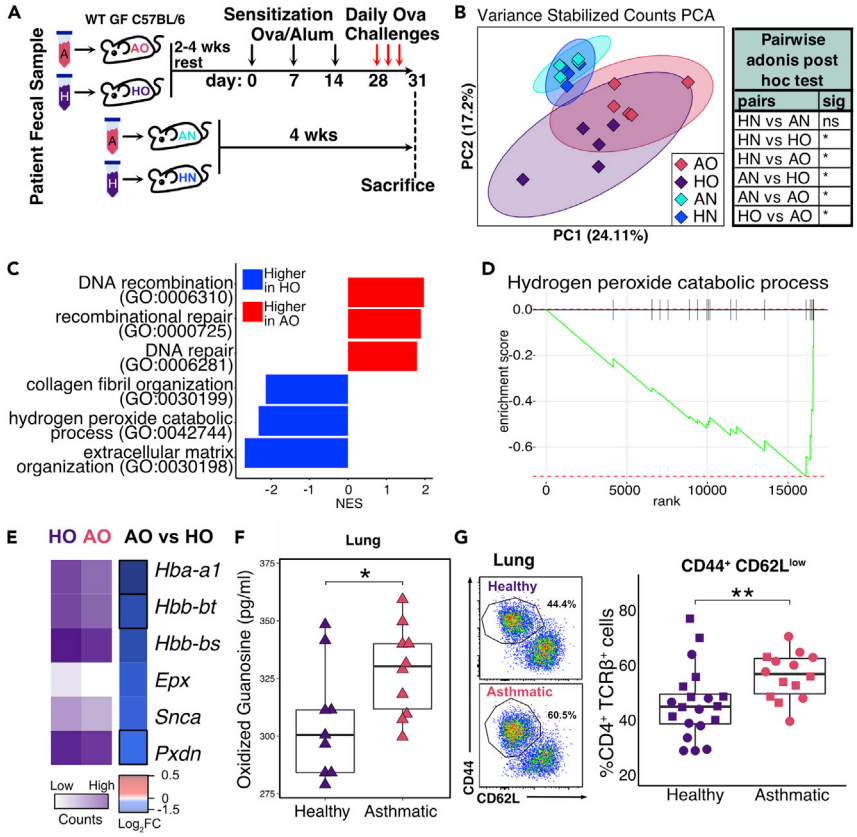

Figure 3. An asthmatic microbiota alters allergic airway inflammation phenotype in humanized gnotobiotic mice

The panels combine four different experiments shown denoted by shape.

(A) Overview of experimental paradigm. O: recipients of ovalbumin sensitization and challenge (OSC); N: no ovalbumin sensitization or challenge; A: recipient of fecal sample from human donor with asthma; H: recipient of healthy donor fecal sample.

(B) Principal Components Analysis of variance-stabilized gene counts from lung RNA-Seq (n = 4,5). (PERMANOVA, 999 permutations: OSC ($p = 0.001$), donor ($p = 0.022$), and donor:OSC interaction ($p = 0.037$); Results of a post-hoc test are also shown in the table.

(C) Bar plot showing normalized enrichment score (NES) of select GO pathways upregulated (red) or down-regulated (blue) in AO mice compared to HO mice (n = 5) (p-adjusted<0.05).

(D) GSEA enrichment plot of the hydrogen peroxide catabolic process pathway upregulated in the lungs of AO mice compared to HO mice.

(E) Heatmap of individual hydrogen peroxide catabolic process genes in AO and HO mice. In purple scale: log-transformed size factor normalized counts. In blue-red scale: Log-2 fold change of AO compared to HO. Genes outlined in black represent a $p < 0.05$.

(F) Oxidized guanosine in AO and HO mouse lungs (n = 9–10 mice per group; Wilcoxon, one-tailed).

(G) Flow cytometry of the lungs of AO and HO mice comparing effector T-cells ($CD44^{+}CD62L^{low}$, CD4+$TCRb^{+}$) from the lungs of AO and HO mice (n = 6–10 mice/group). All experiments include 2–5 males and 2–5 females per group. Shapes denote four separate experiments and are consistent with subsequent figure.

See also Figures S3, S4, and S5.

include hemoglobin synthesis genes (*Hba-a1*, *Hbb-bt*, and *Hbb-bs*), which are known to be upregulated and protective during oxidative stress in extra-erythropoietic tissues,[36,37] and peroxidasin (*Pxdn*), an enzyme which is likewise known to play a protective role during oxidative conditions in tissues (Figure 3E).[38] When considered with the known roles of oxidative stress in upregulating DNA damage and repair machinery in AAI,[39,40] we hypothesized that increased oxidative stress led to DNA damage in AO mice. To test this idea, we measured oxidized guanosine, a marker for oxidative stress,[41] in the lung tissue, and found it to be increased in AO compared to HO groups (Figure 3F). Together, these data reflect increased oxidative stress in the lungs of mice that received the asthmatic microbiota in the context of airway inflammation.

We further investigated the impact of the microbiota on immune cell subsets by performing immunophenotyping on tissues from HO and AO mice. Flow cytometry of lung tissue demonstrated an increase in effector T cells in AO mice compared to HO mice ($TCR\beta^+CD4^+CD62L^{lo}CD44^+$ cells; Figure 3G). Consistent with RNA-Seq results, we did not observe a difference in neutrophils or eosinophils recovered from the lung tissue (Figures S5A and S5B). However, we observed an increase in $CD4^+$ T cells expressing IL-17A after restimulation and intracellular staining (Figure S5C). Coupled with the increased transcription of *Il17a* in the lung tissues (Figure S4B), these findings are consistent with enhanced Th17 cell recruitment to the lungs of AO mice compared to HO mice. This increased Th17 response could also be detected in the mesenteric lymph nodes of AO mice but we did not observe systemic increases in Th17 cells in the spleen or increased serum IL-17A protein (Figures S5C–S5E), suggesting the presence of Th17 cells in the gut and the lung. Taken together, these results support the idea that the gut microbiota from our selected dyad did not change the expression of allergy-associated pathways but did demonstrate alterations in Th17 responses and increased markers of oxidative stress in the lungs of OSC treated mice.

IgA-seq identifies enterotoxigenic *B. fragilis* as a potential effector taxon during AAI

Based on other studies finding that IgA-coated bacteria modulate the host mucosal immune response,[42] we used a technique called IgA-seq to identify microbes from the fecal microbiota that are coated with IgA. Our IgA-seq analysis showed that *Bacteroides* species were more likely to be coated by IgA in AO mice compared to HO mice (Figures 4A and 4B). In AO mice, these IgA-coated bacteria included *B. uniformis* and most prominently, *B. fragilis*. Supported by the observation that *B. fragilis* was in the top 25% of the most discriminatory taxa in the NBC, we isolated and sequenced the *B. fragilis* strain found in the asthmatic microbiota, referred to here as BFM04319. We found that its genome encoded for the *B. fragilis* toxin gene, *bft*, also called fragilysin.

Fragilysin is a *B. fragilis* diarrheal toxin[43] whose proteolytic activity is directed against the adherens junction protein E-cadherin and disrupts the intestinal epithelial barrier.[44,45] We reasoned that gut barrier function would be impaired in AO mice, so we assessed FITC-Dextran leakage in the humanized gnotobiotic mice and found a trend toward increased intestinal permeability in mice colonized with the asthmatic microbiota as early as one week after gavage that persists after OSC (Figure 4C). Similar to previous studies,[46] increased FITC-Dextran leakage was also accompanied by downregulation of the gene encoding for occludin (*Ocln*), an important protein involved in the regulation of intestinal tight junctions, in the colons of AO mice (Figure 4D).

Because gut barrier dysfunction has been previously implicated in inducing systemic oxidative stress,[46,47] we hypothesized that ETBF in our asthmatic stool sample was responsible for the increased oxidative stress in the lungs of AO mice by disrupting the gut barrier. We directly tested whether ETBF alone is sufficient to modulate oxidative stress after OSC by examining three groups of gnotobiotic mice: (1) Mice that remained germ-free (GF); (2) mice monocolonized with BFM04319 (ETBF), and (3) mice monocolonized with a non-toxigenic *B. fragilis* strain VPI2553 (NTBF) (Figure 5A).[48] We performed OSC on all three groups and confirmed that all groups had increases in anti-ovalbumin IgE and Th2 cytokine expression, with the exception of *Il4*, compared to naive germ-free controls providing evidence that we successfully induced AAI (Figures S6A and S6B). We note that IL-4 from whole lung tissues in C57 BL6 mice is a less sensitive measure of AAI than other markers such as IL-5 or IL-13.[49,50] There were no differences in these markers between OSC groups. As expected, mice colonized with ETBF had greater intestinal permeability than either GF controls or NTBF colonized mice (Figure 5B). We observed higher levels of oxidized guanosine in the lungs of ETBF colonized mice compared to GF controls ($p = 0.018$), a trend for NTBF colonized mice to have greater lung oxidized guanosine than GF mice ($p = 0.15$), as well as a trend for ETBF colonized mice to have higher levels of lung oxidized guanosine than NTBF colonized mice ($p = 0.1$, Figure 5C). Furthermore, mice colonized with ETBF had lower neutrophil counts in their bronchoalveolar lavage compared to NTBF-colonized mice or GF controls, although eosinophils, lymphocytes, alveolar macrophages and *Il17a* transcription were not significantly different (Figures 5D and S6B). These results provide evidence that colonization with ETBF is sufficient to cause gut barrier dysfunction, modulate airway inflammatory profile, and increase oxidative stress following OSC.

Expression of *bft* in mice humanized with ETBF+ donor microbiota is highly dependent on microbial community context

Following our identification of ETBF as an important driver of oxidative stress in the lungs of gnotobiotic mice undergoing OSC, we then sought to investigate the importance of ETBF in the context of different

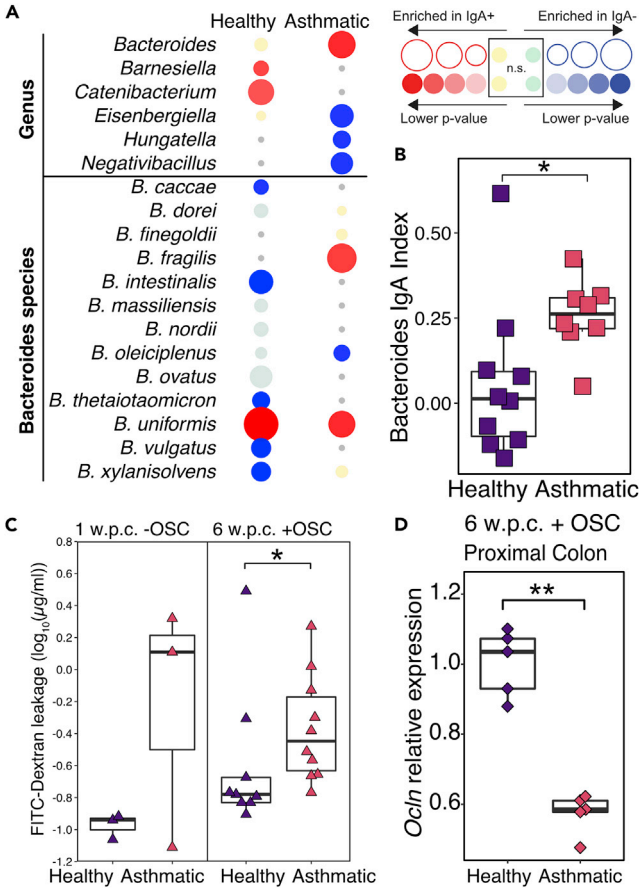

Figure 4. Enterotoxigenic *Bacteroides fragilis* from human donor with asthma is linked to increased gut barrier permeability in humanized gnotobiotic mice

(A) Bubble plot of IgA-Seq results from AO and HO mice at the genus level (n = 8–10 mice/group), and specific species of *Bacteroides*. Bubble color indicates significant enrichment (red) or depletion (blue) in the IgA coated fraction. Bubble size indicates the magnitude of enrichment as determined by the IgA index.

(B) IgA Index of Bacteroides genus between AO mice and HO mice colonized with asthmatic or healthy microbiota (Wilcoxon p = 0.012; n = 8,10 mice/group).

(C) Intestinal permeability of mice colonized with asthmatic and healthy microbiota following a 1-week (Wilcoxon p = 0.7; n = 3 females/group) and 6-week colonization (Wilcoxon p = 0.03; n = 8–10 mice/group) on a log10 scale.

(D) qPCR of occludin gene (*Ocln*) in the proximal colon of humanized mice (Wilcoxon p = 0.008; n = 5 mice/group). All experiments include 4–5 males and 4–5 females per group unless otherwise stated. Shapes denote separate experiments and are consistent with previous figure.Two-sided Wilcoxon test for all boxplots.

See also Figures S3 and S4.

microbial communities. Although exploring multiple donors does not guarantee translatability to humans,[32] it does reveal the strength and robustness of the ETBF-oxidative stress phenotype. Therefore, we selected multiple dyads made up of one ETBF+ donor with asthma and one ETBF-healthy donor for humanization and measured gut barrier permeability, lung cytokine gene expression, and pulmonary oxidative stress after OSC. To select donor samples, we screened MARS stool samples for *bft* using PCR and qPCR[51,52] and identified five asthmatic fecal samples harboring ETBF and five healthy fecal samples lacking ETBF, each pair matched by both age group and community composition metrics derived from our NBC (see STAR Methods; Figures S7A, S7B and Table S1C). Using the selected communities, we humanized germ-free mice and performed OSC. We evaluated humanization in recipient gnotobiotic mice by comparing the Bray-Curtis dissimilarity scores from 16S rRNA sequencing of stool from human donors and recipient mice at the time of sacrifice. This led us to exclude three groups of humanized mice (2 ETBF-, 1 ETBF+) whose engrafted fecal microbiome did not best reflect their donors, leaving seven humanized mouse groups (Figures 6A and S7C; see STAR Methods). As previously observed, all experimental mice

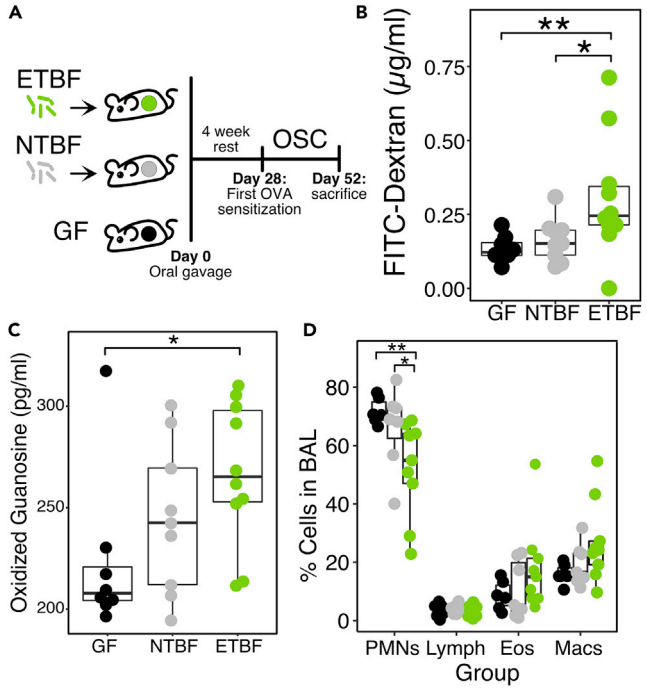

Figure 5. Monocolonization with ETBF increases gut barrier permeability and lung oxidative stress in gnotobiotic mice

(A) Overview of the experimental paradigm testing the ability of *bft* carrying enterotoxigenic *B. fragilis* (ETBF) and *bft* lacking non-toxigenic *B. fragilis* (NTBF) to affect gut barrier function in mice.

(B) Intestinal permeability of mice colonized with either ETBF or NTBF and germ-free controls (GF) (n = 8–10 mice/group; Kruskal-Wallis, one-tailed Dunn post hoc with Benjamini-Hochberg correction).

(C) Oxidized guanosine in lungs of ETBF, NTBF, and GF mice (n = 8–10 mice/group; Kruskal-Wallis, one-tailed Dunn post hoc with Benjamini-Hochberg correction).

(D) Cytospin cell counts from bronchoalveolar lavage collected from mice colonized with ETBF, NTBF or germ-free controls. PMN = polymorphonuclear cells (i.e. neutrophils), Lymph = lymphocytes, Eos = eosinophils, Mac = macrophages (n = 8–10 mice/group; Kruskal-Wallis, one-tailed Dunn post hoc with Benjamini-Hochberg correction). This experiment includes 3–4 males and 5–7 females per group.

See also Figure S6.

had increases in Th2 cytokine expression, except *Il4*, and anti-ovalbumin IgE compared to naive germ-free controls and that there were no differences in these markers between OSC groups (Figures S7D and S7E).

Overall, we found no differences in gut barrier leakage, pulmonary oxidative stress, or gene expression of lung cytokines between mice colonized with an asthmatic ETBF+ microbiota and those receiving an ETBF- healthy microbiota (Figures S7E–S7G). To understand the differences between these experiments and our original donor experiment, we measured copies of *bft* RNA and DNA in the cecal contents of ETBF+ humanized mice and found that the median expression levels of the mice with newly selected human samples were 1.2- to 67.5-fold lower than that of the original donor sample, MARS0043 (Figure 6B, t-test p = 0.01). These results are consistent with previous research showing that ETBF vary their enterotoxin expression based on the microbial community context[53] and may explain the lack of an ETBF-oxidative stress phenotype seen in these mice.

Given that the expression of *bft* was far more variable than observed in the original donor dyad, we tested if there was any correlation between *bft* expression and markers of Th17 or AAI. As expected, the expression of Th2 cytokine encoding genes *Il5* and *Il13* were highly correlated with each other in both experimental groups. However, we found that *Il5* and *Il13* were correlated with *Il4* in mice colonized with ETBF- microbiota from healthy individuals, but not in mice colonized with ETBF+ microbiota from individuals with asthma (Figure 6C). The *Il4*/*Il5* and *Il4*/*Il13* correlations observed in the healthy group were significantly stronger than that in the asthma group (Steiger's test p = 0.0044 and 0.0026 respectively), suggesting

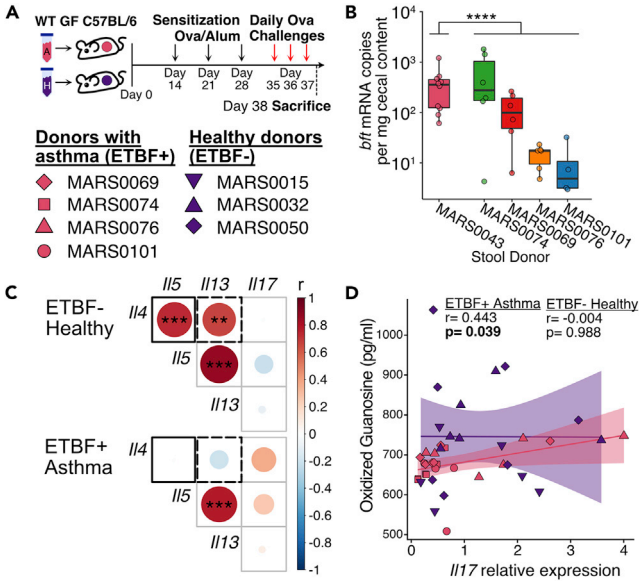

Figure 6. Humanization with multiple microbiota suggests ETBF produced *bft* can alter lung inflammation in a community context dependent manner

(A) Overview of experimental paradigm. Five healthy and five asthmatic donor microbiota were used to humanize germ-free mice (4–7 mice per donor). Two weeks later, pulmonary inflammation was induced by OSC. After evaluating humanization, only seven mouse groups were used in subsequent analyses.

(B) qPCR measurements of *bft* in the cecal content of humanized mice (t-test against initial MARS0043 microbiome).

(C) Pearson correlations between RT-qPCR measures of lung cytokines from mice humanized by ETBF- healthy (top) and ETBF+ asthmatic (bottom) microbiota. Area and color of the circle represent the absolute value of the Pearson correlation coefficient with corresponding color key. Asterisks represent the p value from the Pearson correlation. Solid (Steiger's test; p = 0.0044) and dotted (Steiger's test; p = 0.0026) black squares indicate a statistically significant difference between the two outlined correlations.

(D) Pearson correlation between oxidized guanosine in the lungs of humanized mice and RT-qPCR measures of lung *Il17*. All experimental groups included 1–4 female and 2–4 male mice.

See also Figure S7.

different patterns of Th2 cytokine expression in the lungs. Previous studies have identified a correlation between *Il17* expression and oxidative stress in the lungs.[5] We found that ETBF+ humanized mice displayed the expected correlation between lung *Il17a* expression and oxidative stress (Figure 6D, Pearson = 0.443, p = 0.039), but the ETBF-healthy humanized mice did not (Pearson = −0.004, p = 0.987). Together, these results suggest that ETBF+ microbiota from donors with asthma may link oxidative stress to *Il17a*.

Gut colonization with ETBF is more prevalent among individuals with asthma compared to healthy controls

Finally, we investigated the importance of *bft* in humans by examining its prevalence in the stool of MARS participants. Using PCR and qPCR,[51,52] we screened all human fecal specimens in which *B. fragilis* was detected by 16S rRNA sequencing for *bft* and found a total of eight individuals with asthma and two healthy subjects with detectable *bft*. Though prevalent in only 22% of the asthma cohort, *bft* is significantly enriched in subjects with asthma compared to healthy individuals (Figures 7A and 2B). There was no statistically significant difference in Asthma Control Test score[54] between patients with or without ETBF (Table S1D, p = 0.3). We then asked whether higher rates of ETBF could be a consequence of an increased prevalence of *B. fragilis* in the asthma cohort but found no difference in the frequency of *B. fragilis* colonization (Figure 7B). Even among only individuals colonized with *B. fragilis*, patients with asthma were still more likely to be colonized with ETBF than NTBF compared to healthy individuals (Figure 7C). We next examined fecal calprotectin levels from remaining subjects to determine whether asthma was associated with gut barrier permeability. Overall, we found that calprotectin was either low or undetectable in all samples but tended to be more detectable in samples originating from a donor with asthma (Fisher's test p value = 0.053, Figure 7D). Although the low levels of calprotectin are likely because of long-term sample storage, these results tentatively suggest a degree of barrier dysfunction in patients with asthma.

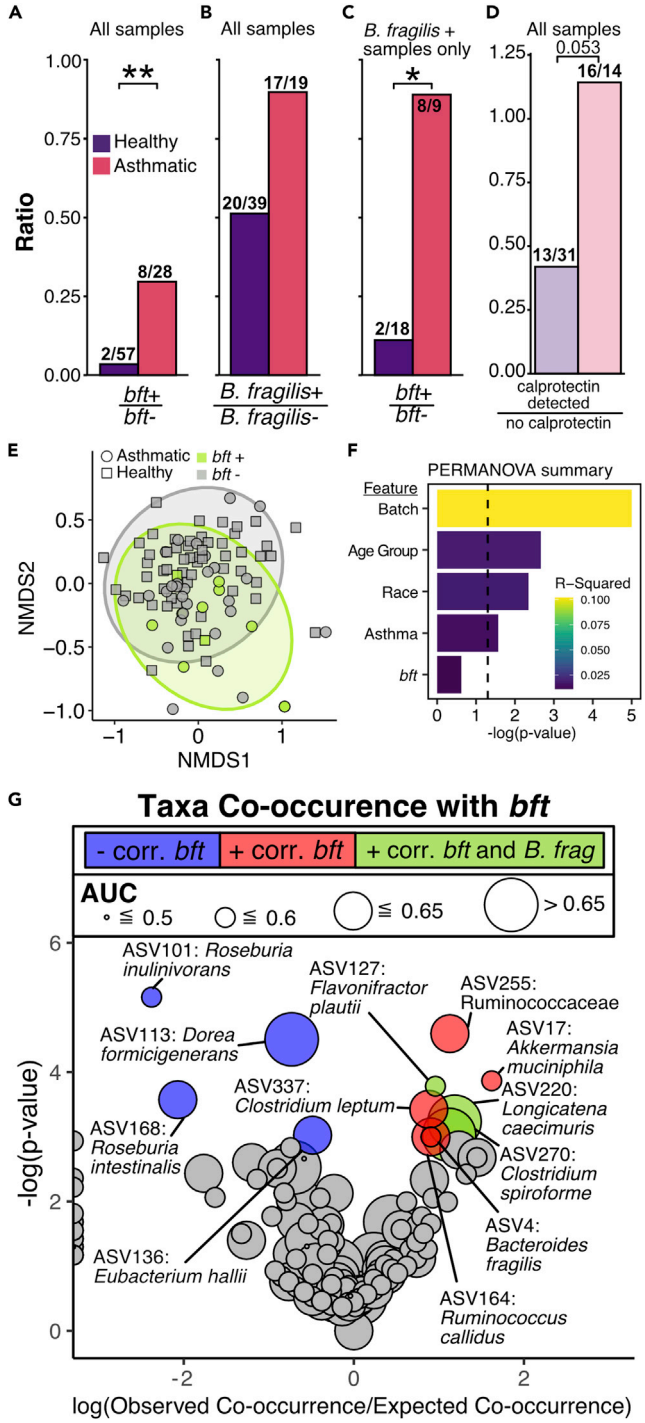

Figure 7. *bft* is enriched in individuals with asthma

(A–D) Ratios of (A) *bft* positive over *bft* negative samples (n = 59 Healthy, 36 Asthmatic). *bft* positive samples were characterized by PCR and qPCR screening among the 37 total subjects with *B. fragilis*. The 58 remaining subjects without *B. fragilis* by 16S rRNA sequencing were not screened and were considered *bft* negative. (B) *B. fragilis* positive samples over *B. fragilis* negative samples, characterized by V4 16S rRNA community profiling (n = 59 Healthy, 36 Asthmatic). (C) *bft* positive samples with *B. fragilis* over *bft* negative samples with *B. fragilis* (n = 20 Healthy, 17 Asthmatic). (D) Stool samples with detectable calprotectin via ELISA over those with no detectable calprotectin.

Figure 7. *Continued*

(E) Non-metric multidimensional scaling (NMDS) on Bray-Curtis dissimilarity of MARS donor microbiomes at ASV-level. Ellipses represent 95% confidence intervals. Shape denotes asthma (circle) or healthy (square). Color denotes a positive (green) or negative (gray) hit for *bft* in fecal gDNA.

(F) Bar plot summarizing results of a sequential PERMANOVA analysis on the beta diversity in (E). Color represents R^2 value and the length of the bar represents-log(p value). Dashed line indicates a p value threshold of 0.05.

(G) Volcano plot describing co-occurrence between *bft* and taxa in human stool samples, calculated as the log ratio of the number of samples in which *bft* was observed in the same sample as the taxon compared to the number of times *bft* and the taxon would be expected to occur in the same sample by chance alone.[55] Color represents a significant positive (red) or negative (blue) co-occurrence with *bft* after multiple hypothesis correction. Taxa positively correlated with *bft* and *B. fragilis* (ASV4) are shown in green. Gray represents a non-significant relationship. Size represents the area under the ROC curve (AUC) of the taxa calculated from the NBC. (For all panels except C and D: n = 59 Healthy, 36 Asthmatic).

See also Figure S1.

To check if *bft* presence alone associated with a shift in the microbiota as a whole, we tested *bft* presence as a feature in a sequential PERMANOVA on Bray-Curtis beta diversity (Figure 7E) after accounting for the important demographics presented in Figure 1C (sequencing batch, race, age, and asthma status). We found no statistically significant effect of *bft* presence alone on global shift in the beta diversity (p = 0.24; Figure 7F). However, we suspected that other taxa in the gut may be associated with ETBF, so we performed a co-occurrence analysis with *bft* presence and our 16S rRNA sequencing results (Figure 7G). In addition to *B. fragilis*, we identified 7 taxa positively correlated and 4 negatively correlated with ETBF colonization. Among the positively correlated taxa were 4 taxa that co-occurred with *bft* but not *B. fragilis* (ASV4), suggesting that ETBF may influence gut microbiota composition in a different manner from NTBF species. Notably, *bft* co-occurs with *Dorea formicigenerans* (ASV113, AUC = 0.663, Rank 11), *L. caecimuris* (ASV220, AUC = 0.662, Rank 12), and *Clostridium spiroforme* (ASV270, AUC = 0.657, Rank 13), which are highly discriminatory between asthma and healthy individuals according to our NBC (Figure S8A). In addition, our differential abundance analysis of ETBF+ microbiota against ETBF- microbiota, identified enrichment of *C.spiroforme* (ASV270, AUC = 0.657, Rank 13) and *Ruminococcaceae* (ASV255, AUC = 0.628, Rank 29) in the ETBF+ donors and *R. intestinalis* (ASV168, AUC = 0.602, Rank 65) in the ETBF- donors, supporting the findings from the co-occurrence analysis (Table S3). These results imply that the presence of *bft* reinforces asthma-associated changes in the gut microbiota.

DISCUSSION

Despite our growing understanding of the origins of asthma, the heterogeneous nature of the disease remains a barrier to treatment. In addition to factors such as age,[56] sex,[57] smoking status,[58] and microbial exposures,[59] the gut microbiota is increasingly appreciated as a determinant of asthma risk.[10,34] Here we leverage a cross-sectional human clinical study of 95 patients with and without asthma and use humanized gnotobiotic mice to show that, in the right community context, ETBF can increase Th17 inflammation and oxidative stress in the lungs of mice with AAI, potentially by disrupting the gut barrier. This finding is of potential clinical relevance because we found that ETBF is more prevalent in the gut microbiomes of people with asthma.

Humanization of gnotobiotic mice is a powerful tool to study the human microbiota and its effects on host phenotypes, but has many well-established caveats. First, the human microbiota does not perfectly maintain community and functional structure between donors and mouse recipients.[32,60] Second, virulence factors adapted to human hosts may not affect mice to the same degree. Third, a gut microbiota may influence the host phenotype by multiple mechanisms simultaneously, such as in asthma where multiple microbial metabolites are known to alter the course of the disease, each by their own respective mechanisms.[10,12–14] Together, these issues can complicate the interpretation of results from gnotobiotic experiments and affect the translatability of those results back to humans.

Designing experiments to address these limitations requires the selection of donor samples that both control for confounding factors that modify the microbiome apart from the disease of interest as well as capture the relevant microbial relationships between healthy and disease-affected populations. Control of confounding factors is often accomplished by matching the clinical demographics of donors[32,61] (Figures 1B and 1C) but there is no standardized practice for identifying samples that capture important microbial relationships. Given the immense interpersonal variability of the microbiome,[62–64] no single pair of samples captures all the discriminatory microbial features from a population but we can still select

pairs enriched in these relationships to study. We believe that the approach presented here for sample selection will be useful in identifying microbial drivers of disease in future clinical studies.

Our in-depth profiling of a single dyad revealed an ETBF+ microbiome from a donor with asthma increased the Th17 response and oxidative stress within the lungs of humanized gnotobiotic mice in the context of AAI. Although previous studies have implicated airway microbes in inducing Th17 responses in AAI,[27,65] our work provides evidence that this phenotype can be mediated by a gut microbiota-expressed factor. In follow-up monocolonization experiments, we confirmed that the ETBF isolated from the donor with asthma causes increased gut barrier permeability and pulmonary oxidative stress in the context of pre-existing inflammation. Intriguingly, we observed that neutrophils were lower in ETBF colonized mice, implying that the increased oxidative stress is not a result of reactive oxygen species generation from neutrophils. On the other hand microbial products, including LPS and fragilysin, have been shown to directly induce oxidative damage in lung and gut epithelial cells, respectively,[66,67] suggesting an alternative source of oxidative stress. Notably, we did not measure an increased Th17 response in the lungs of ETBF monocolonized mice compared to NTBF or GF mice. This could mean that other community members in addition to ETBF are important for inducing systemic[68] and lung Th17 responses.

We also explored the effect of community context on ETBF by colonizing groups of mice with ETBF+ communities from multiple donors with asthma. We did not detect increased gut permeability, pulmonary oxidative stress, or lung Th17 responses in the ETBF+ humanized mice. However, we did observe that overall expression of *bft* was much lower in this experiment compared to the MARS0043. Despite this, ETBF+ asthmatic microbiota caused an altered pattern of Th2 cytokine expression compared to ETBF-healthy microbiota. Taken with our ETBF monocolonization data, these results imply that *bft* may influence inflammation in the lungs, but that its expression and impact on asthma may be modulated by community context. Based on these results, we propose that *bft* and ETBF may contribute to the clinical heterogeneity of asthma in humans and raise the question of whether additional gut microbes may contribute to asthma endotype.

Although gnotobiotic experiments offer control over many features of the gut microbiota, they ultimately remain a proxy of asthma in humans. Confirming the findings from our humanized mouse models will require a longitudinal human clinical study including ETBF colonized subjects with asthma and controls that undergo rigorous phenotypic characterization that incorporates measuring gut barrier permeability, circulating microbial products, and immunophenotyping of the blood and bronchial lavage. The results of this study would establish whether ETBF could adversely influence asthma in people and define the environmental and microbial circumstances that enable ETBF to cause these phenotypes. In addition, the outcomes of such a clinical study could also link two previously disparate features of asthma: first, that increased gut permeability[69,70] and increased gastrointestinal symptoms[71] have been observed in patients with asthma, and secondly, that increased oxidative stress is associated with more severe asthma with a higher rate of exacerbations and corticosteroid resistance.[72,73]

We acknowledge that ETBF is unlikely to be a universal mechanism contributing to asthma and would probably only apply to a subset of people living with asthma (22% from our study). We also observed in our mouse models that the effects of ETBF were highly variable and caused barrier permeability and increased pulmonary oxidative stress in only one of the six ETBF+ microbiota samples we tested from individuals with asthma. These results came from four different colonization experiments (Figures 3 and 4) using the first human donor dyad before the experiment that employed ten human donors (Figure 6), strongly supporting a distinct effect of the initial donor dyad on AAI. The first set of experiments replicated an effect on lung inflammation associated with ETBF colonization in AAI, whereas the second set of experiments demonstrates that this phenotype is not generalizable to all of the ETBF+ donors. It could be the case that, like ETBF-induced weight loss, the gut and lung phenotypes caused by the one ETBF+ microbiota sample opportunely emerge in particular community and environmental contexts (Figures 6 and S7).[53] Here, we suspect that other members of the gut microbiota are important for *bft* expression and substantially modulate the penetrance of the ETBF phenotype on AAI. For example, *Roseburia* species, linked to protective effects in AAI,[21] tend not to cooccur with ETBF in our study whereas *Ruminococcus* species including *R. callidus* that cooccur with ETBF have been found to be enriched in the stool of patients with asthma.[55]

On the other hand, implicating a barrier-disrupting organism in asthma pathology could lead to unique interventions to improve asthma control. For instance, targeting ETBF colonization by vaccination,

antibiotics, or phage therapy could offer a novel means of manipulating the immune manifestations of asthma. Alternatively, candidate therapeutics designed to improve gut barrier function through their effects on tight junctions for other diseases including arthritis[74] and celiac disease[75] could be repurposed to modify the gut-lung axis in asthma. Unlike early childhood interventions that aim to alter the development of asthma, these therapies may provide benefit to patients with established disease.

Limitations of the study

Because our cross-sectional study focused on patients with established disease, we cannot demonstrate a causal relationship between ETBF or the gut microbiota and asthma. Rather, our findings demonstrate that ETBF modifies the immunological characteristics of the lung in gnotobiotic mice experiencing AAI. We identified these findings by contrasting microbiota sourced from healthy donors against stool sourced from patients with asthma, but our findings are limited in that we cannot separate the effects of the rest of the microbiota. Although this could be accomplished by testing microbiota from subjects with asthma that contain ETBF against microbiota from asthma subjects without ETBF, based on our data from Figure 6, we estimate that the number of samples we need to separate the effect of ETBF from other microbes exceeds the number available from our clinical study. In our experiments, we intentionally chose the ovalbumin-alum model because it is a well-characterized antigen that is easily translated into gnotobiotic models. Ovalbumin does not evoke the strongest AAI response in C57 BL6 mice,[49,50] as we observed for *Il4* in our study, and future gnotobiotic experiments will need to include a broader range of biologically relevant antigens such as house dust mite or cockroach antigen to better contextualize our findings in acute mouse AAI to human asthma, a chronic disease. In addition, humanized gnotobiotic experiments are limited by the level of engraftment of donor microbes and the differences between human and mouse host biology. Although we could reduce variation because of engraftment in some experiments by performing multiple replicates (e.g. Figure 3), it was not technically feasible for us to perform this on all experiments given the challenges inherent to gnotobiotic experiments. Future studies extrapolating our results to other strains and microbiota would further contextualize our findings, but ultimately the mechanistic insights revealed by these models must be confirmed in clinical studies.

STAR★METHODS

Detailed methods are provided in the online version of this paper and include the following:

- KEY RESOURCES TABLE
- RESOURCE AVAILABILITY
  - Lead contact
  - Materials availability
  - Data and code availability
- EXPERIMENTAL MODEL AND SUBJECT DETAILS
  - Human subjects
  - Experimental animals and ethics
  - Isolation and growth *Bacteroides fragilis* strains
- METHOD DETAILS
  - Humanized gnotobiotic mouse model
  - Allergic airway inflammation model
  - Processing of stool and 16S rRNA profiling library preparation
- ANALYSIS OF 16S RRNA DATA
  - IgA-seq
  - Whole genome sequencing of BFM04319
  - Immune cell isolation from tissues
  - Flow cytometry of isolated immune cells
  - Transcriptional profiling of mouse lungs
  - Lung RT-qPCR
  - Protein quantification
  - DNA/RNA oxidative damage ELISA
  - Intestinal permeability assay
  - Cytospin
  - Screening for bft in subject stool samples
  - Quantitation of bft expression in mouse cecal contents
  - Quantitation of calprotectin in human stool samples

- QUANTIFICATION AND STATISTICAL ANALYSIS
  - Statistics
  - Mixture distribution Naïve Bayes' classifier for 16S profiling of asthma vs. healthy patients

SUPPLEMENTAL INFORMATION

Supplemental information can be found online at https://doi.org/10.1016/j.isci.2023.105991.

ACKNOWLEDGMENTS

We would like to thank our clinical study coordinators Tarisa Mantia, Caitlin O'Shaughnessy, and Shannon Rook; the physicians of Washington University Pediatric and Adolescent Ambulatory Research Consortium, especially Dr. Jane Garbutt; the Volunteer for Health registry; and the MARS participants and their families. We would also like to acknowledge Dr. Devesha Kulkarni, for her technical expertise as well as the Center for Genome Sciences Sequencing Core and Genome Technology Access Center at the McDonnell Genome Institute for sequencing services. The authors also thank Drs. Brain Laidlaw and Leyao Wang for critical reading of the manuscript and Drs Philip Ahern, Neelendu Dey, and Ansel Hsiao for thoughtful feedback on our work. A.L.K. is funded by the AAAAI Foundation Faculty Development Award and the NIH K08 AI113184. A.H-L received funding through the NIH T32 GM007200 and F30 DK127584. J.S-B received funding through the NIH T32 GM007067.

AUTHOR CONTRIBUTIONS

N.G.W., A.H.-L., and A.L.K. conceptualized the work. L.B.B. and A.L.K. planned the clinical study. N.G.W., A.H.-L., A.L.R., N.J., R.T.M., J.S.-B., M.A.L., C.P.T. and A.L.K. contributed to the design and conduct of experiments. N.G.W., A.H.-L., A.L.R., N.J., R.T.M., and A.L.K. analyzed the data. N.G.W., A.H.-L., T.R.R., and S.J.S. developed gnominator. N.G.W., A.H.-L., and A.L.K. drafted the manuscript. All authors interpreted the data and contributed to revising the manuscript.

DECLARATION OF INTERESTS

The authors have no competing interests to declare.

INCLUSION AND DIVERSITY

One or more of the authors of this paper self-identifies as an underrepresented ethnic minority in their field of research or within their geographical location. One or more of the authors of this paper self-identifies as a gender minority in their field of research. One or more of the authors of this paper self-identifies as a member of the LGBTQIA+ community.

We support inclusive, diverse, and equitable conduct of research.

Received: September 7, 2022
Revised: November 28, 2022
Accepted: January 11, 2023
Published: January 18, 2023

REFERENCES

1. Kaur, R., and Chupp, G. (2019). Phenotypes and endotypes of adult asthma: moving toward precision medicine. J. Allergy Clin. Immunol. *144*, 1–12. https://doi.org/10.1016/j.jaci.2019.05.031.

2. Wenzel, S.E. (2012). Asthma phenotypes: the evolution from clinical to molecular approaches. Nat. Med. *18*, 716–725. https://doi.org/10.1038/nm.2678.

3. Nadif, R., Febrissy, M., Andrianjafimasy, M.V., Le Moual, N., Gormand, F., Just, J., Pin, I., Siroux, V., Matran, R., Dumas, O., and Nadif, M. (2020). Endotypes identified by cluster analysis in asthmatics and non-Asthmatics and their clinical characteristics at follow-up: the case-control EGEA study. BMJ Open Respir.Res. *7*, 0006322–e712. https://doi.org/10.1136/bmjresp-2020-000632.

4. Cho, Y.S., and Moon, H.B. (2010). The role of oxidative stress in the pathogenesis of asthma. Allergy Asthma Immunol. Res. *2*, 183–187. https://doi.org/10.4168/AAIR.2010.2.3.183.

5. Camargo, L.d.N., Righetti, R.F., Aristóteles, L., dos Santos, T.M., de Souza, F.C.R., Fukuzaki, S., Cruz, M.M., Alonso-Vale, M.I.C., Saraiva-Romanholo, B.M., Prado, C.M., et al. (2018). Effects of anti-IL-17 on inflammation, remodeling, and oxidative stress in an experimental model of asthma exacerbated by LPS. Front. Immunol. *8*, 1835. https://doi.org/10.3389/fimmu.2017.01835.

6. Garcia-Nuñez, M., Millares, L., Pomares, X., Ferrari, R., Pérez-Brocal, V., Gallego, M., Espasa, M., Moya, A., and Monsó, E. (2014). Severity-related changes of bronchial microbiome in chronic obstructive pulmonary disease. J. Clin. Microbiol. *52*, 4217–4223. https://doi.org/10.1128/JCM.01967-14.

7. McAleer, J.P., Nguyen, N.L.H., Chen, K., Kumar, P., Ricks, D.M., Binnie, M., Armentrout, R.A., Pociask, D.A., Hein, A., Yu,

A., et al. (2016). Pulmonary Th17 antifungal immunity is regulated by the gut microbiome. J. Immunol. *197*, 97–107. https://doi.org/10.4049/jimmunol.1502566.

8. Fagundes, C.T., Amaral, F.A., Vieira, A.T., Soares, A.C., Pinho, V., Nicoli, J.R., Vieira, L.Q., Teixeira, M.M., and Souza, D.G. (2012). Transient TLR activation restores inflammatory response and ability to control pulmonary bacterial infection in germfree mice. J. Immunol. *188*, 1411–1420. https://doi.org/10.4049/jimmunol.1101682.

9. Gauguet, S., D'Ortona, S., Ahnger-Pier, K., Duan, B., Surana, N.K., Lu, R., Cywes-Bentley, C., Gadjeva, M., Shan, Q., Priebe, G.P., and Pier, G.B. (2015). Intestinal microbiota of mice influences resistance to Staphylococcus aureus pneumonia. Infect. Immun. *83*, 4003–4014. https://doi.org/10.1128/IAI.00037-15.

10. Arrieta, M.-C., Stiemsma, L.T., Dimitriu, P.A., Thorson, L., Russell, S., Yurist-Doutsch, S., Kuzeljevic, B., Gold, M.J., Britton, H.M., Lefebvre, D.L., et al. (2015). Early infancy microbial and metabolic alterations affect risk of childhood asthma. Sci. Transl. Med. *7*, 307ra152. https://doi.org/10.1126/scitranslmed.aab2271.

11. Enaud, R., Prevel, R., Ciarlo, E., Beaufils, F., Wieërs, G., Guery, B., and Delhaes, L. (2020). The gut-lung Axis in health and respiratory diseases: a place for inter-organ and inter-kingdom crosstalks. Front. Cell. Infect. Microbiol. *10*, 9. https://doi.org/10.3389/fcimb.2020.00009.

12. Cait, A., Hughes, M.R., Antignano, F., Cait, J., Dimitriu, P.A., Maas, K.R., Reynolds, L.A., Hacker, L., Mohr, J., Finlay, B.B., et al. (2018). Microbiome-driven allergic lung inflammation is ameliorated by short-chain fatty acids. Mucosal Immunol. *11*, 785–795. https://doi.org/10.1038/mi.2017.75.

13. Levan, S.R., Stamnes, K.A., Lin, D.L., Panzer, A.R., Fukui, E., McCauley, K., Fujimura, K.E., McKean, M., Ownby, D.R., Zoratti, E.M., et al. (2019). Elevated faecal 12,13-diHOME concentration in neonates at high risk for asthma is produced by gut bacteria and impedes immune tolerance. Nat. Microbiol. *4*, 1851–1861. https://doi.org/10.1038/s41564-019-0498-2.

14. Fujimura, K.E., Sitarik, A.R., Havstad, S., Lin, D.L., Levan, S., Fadrosh, D., Panzer, A.R., Lamere, B., Rackaityte, E., Lukacs, N.W., et al. (2016). Neonatal gut microbiota associates with childhood multisensitized atopy and T cell differentiation. Nat. Med. *22*, 1187–1191. https://doi.org/10.1038/nm.4176.

15. Mossad, O., Batut, B., Yilmaz, B., Dokalis, N., Mezö, C., Nent, E., Nabavi, L.S., Mayer, M., Maron, F.J.M., Buescher, J.M., et al. (2022). Gut microbiota drives age-related oxidative stress and mitochondrial damage in microglia via the metabolite N6-carboxymethyllysine. Nat. Neurosci. *25*, 295–305. https://doi.org/10.1038/S41593-022-01027-3.

16. Zhou, W., Wu, W.H., Si, Z.L., Liu, H.L., Wang, H., Jiang, H., Liu, Y.F., Alolga, R.N., Chen, C., Liu, S.J., and Bian, X.Y. (2022). The gut microbe Bacteroides fragilis ameliorates renal fibrosis in mice. Nat. Commun. *13*, 6081. https://doi.org/10.1038/S41467-022-33824-6.

17. Stiemsma, L.T., and Michels, K.B. (2018). The Role of the microbiome in the developmental origins of health and disease. Pediatrics *141*, e20172437. https://doi.org/10.1542/peds.2017-2437.

18. Olin, A., Henckel, E., Chen, Y., Lakshmikanth, T., Pou, C., Mikes, J., Gustafsson, A., Bernhardsson, A.K., Zhang, C., Bohlin, K., and Brodin, P. (2018). Stereotypic immune system development in newborn children. Cell *174*, 1277–1292.e14. https://doi.org/10.1016/j.cell.2018.06.045.

19. Teo, S.M., Tang, H.H.F., Mok, D., Judd, L.M., Watts, S.C., Pham, K., Holt, B.J., Kusel, M., Serralha, M., Troy, N., et al. (2018). Airway microbiota dynamics uncover a critical window for interplay of pathogenic bacteria and allergy in childhood respiratory disease. Cell Host Microbe *24*, 341–352.e5. https://doi.org/10.1016/j.chom.2018.08.005.

20. Abrahamsson, T.R., Jakobsson, H.E., Andersson, A.F., Björkstén, B., Engstrand, L., and Jenmalm, M.C. (2014). Low gut microbiota diversity in early infancy precedes asthma at school age. Clin. Exp. Allergy *44*, 842–850. https://doi.org/10.1111/cea.12253.

21. Depner, M., Taft, D.H., Kirjavainen, P.V., Kalanetra, K.M., Karvonen, A.M., Peschel, S., Schmausser-Hechfellner, E., Roduit, C., Frei, R., Lauener, R., et al. (2020). Maturation of the gut microbiome during the first year of life contributes to the protective farm effect on childhood asthma. Nat. Med. *26*, 1766–1775. https://doi.org/10.1038/s41591-020-1095-x.

22. Begley, L., Madapoosi, S., Opron, K., Ndum, O., Baptist, A., Rysso, K., Erb-Downward, J.R., and Huang, Y.J. (2018). Gut microbiota relationships to lung function and adult asthma phenotype: a pilot study. BMJ Open Respir.Res. *5*, e000324–e000327. https://doi.org/10.1136/bmjresp-2018-000324.

23. Chiu, C.Y., Cheng, M.L., Chiang, M.H., Kuo, Y.L., Tsai, M.H., Chiu, C.C., and Lin, G. (2019). Gut microbial-derived butyrate is inversely associated with IgE responses to allergens in childhood asthma. Pediatr.Allergy Immunol. *30*, 689–697. https://doi.org/10.1111/pai.13096.

24. Barcik, W., Pugin, B., Westermann, P., Perez, N.R., Ferstl, R., Wawrzyniak, M., Smolinska, S., Jutel, M., Hessel, E.M., Michalovich, D., et al. (2016). Histamine-secreting microbes are increased in the gut of adult asthma patients. J. Allergy Clin. Immunol. *138*, 1491–1494.e7. https://doi.org/10.1016/j.jaci.2016.05.049.

25. Michalovich, D., Rodriguez-Perez, N., Smolinska, S., Pirozynski, M., Mayhew, D., Uddin, S., Van Horn, S., Sokolowska, M., Altunbulakli, C., Eljaszewicz, A., et al. (2019). Obesity and disease severity magnify disturbed microbiome-immune interactions in asthma patients. Nat. Commun. *10*, 5711. https://doi.org/10.1038/s41467-019-13751-9.

26. Arrieta, M.C., Sadarangani, M., Brown, E.M., Russell, S.L., Nimmo, M., Dean, J., Turvey, S.E., Chan, E.S., and Finlay, B.B. (2016). A humanized microbiota mouse model of ovalbumin-induced lung inflammation. Gut Microb. *7*, 342–352. https://doi.org/10.1080/19490976.2016.1182293.

27. Jaeger, N., McDonough, R.T., Rosen, A.L., Hernandez-Leyva, A., Wilson, N.G., Lint, M.A., Russler-Germain, E.V., Chai, J.N., Bacharier, L.B., Hsieh, C.-S., and Kau, A.L. (2020). Airway microbiota-host interactions regulate Secretory leukocyte protease inhibitor levels and influence allergic airway inflammation. Cell Rep. *33*, 108331. https://doi.org/10.1016/j.celrep.2020.108331.

28. Callahan, B.J., McMurdie, P.J., Rosen, M.J., Han, A.W., Johnson, A.J.A., and Holmes, S.P. (2016). DADA2: high-resolution sample inference from Illumina amplicon data. Nat. Methods *13*, 581–583. https://doi.org/10.1038/nmeth.3869.

29. Laigaard, A., Krych, L., Zachariassen, L.F., Ellegaard-Jensen, L., Nielsen, D.S., Hansen, A.K., and Hansen, C.H.F. (2020). Dietary prebiotics promote intestinal Prevotella in association with a low-responding phenotype in a murine oxazolone-induced model of atopic dermatitis. Sci. Rep. *10*, 21204–21211. https://doi.org/10.1038/s41598-020-78404-0.

30. Larsen, J.M. (2017). The immune response to Prevotella bacteria in chronic inflammatory disease. Immunology *151*, 363–374. https://doi.org/10.1111/imm.12760.

31. Chua, H.H., Chou, H.C., Tung, Y.L., Chiang, B.L., Liao, C.C., Liu, H.H., and Ni, Y.H. (2018). Intestinal dysbiosis featuring abundance of Ruminococcus gnavus associates with allergic diseases in infants. Gastroenterology *154*, 154–167. https://doi.org/10.1053/j.gastro.2017.09.006.

32. Walter, J., Armet, A.M., Finlay, B.B., and Shanahan, F. (2020). Establishing or exaggerating causality for the gut microbiome: lessons from human microbiota-associated rodents. Cell *180*, 221–232. https://doi.org/10.1016/j.cell.2019.12.025.

33. Dzidic, M., Abrahamsson, T.R., Artacho, A., Björkstén, B., Collado, M.C., Mira, A., and Jenmalm, M.C. (2017). Aberrant IgA responses to the gut microbiota during infancy precede asthma and allergy development. J. Allergy Clin. Immunol. *139*, 1017–1025.e14. https://doi.org/10.1016/j.jaci.2016.06.047.

34. Trompette, A., Gollwitzer, E.S., Yadava, K., Sichelstiel, A.K., Sprenger, N., Ngom-Bru, C., Blanchard, C., Junt, T., Nicod, L.P., Harris, N.L., and Marsland, B.J. (2014). Gut microbiota metabolism of dietary fiber influences allergic airway disease and hematopoiesis. Nat. Med. *20*, 159–166. https://doi.org/10.1038/nm.3444.

35. Vael, C., Nelen, V., Verhulst, S.L., Goossens, H., and Desager, K.N. (2008). Early intestinal Bacteroides fragilis colonisation and development of asthma. BMC Pulm. Med. *8*, 19–26. https://doi.org/10.1186/1471-2466-8-19.

36. Nishi, H., Inagi, R., Kato, H., Tanemoto, M., Kojima, I., Son, D., Fujita, T., and Nangaku, M. (2008). Hemoglobin is expressed by mesangial cells and reduces oxidant stress.

J. Am. Soc. Nephrol. *19*, 1500–1508. https://doi.org/10.1681/ASN.2007101085.

37. Liu, W., Baker, S.S., Baker, R.D., Nowak, N.J., and Zhu, L. (2011). Upregulation of hemoglobin expression by oxidative stress in hepatocytes and its implication in nonalcoholic steatohepatitis. PLoS One *6*, e24363. https://doi.org/10.1371/journal.pone.0024363.

38. Dougan, J., Hawsawi, O., Burton, L.J., Edwards, G., Jones, K., Zou, J., Nagappan, P., Wang, G., Zhang, Q., Danaher, A., et al. (2019). Proteomics-metabolomics combined approach identifies peroxidasin as a protector against metabolic and oxidative stress in prostate cancer. Int. J. Mol. Sci. *20*, 3046. https://doi.org/10.3390/ijms20123046.

39. Chan, T.K., Loh, X.Y., Peh, H.Y., Tan, W.N.F., Tan, W.S.D., Li, N., Tay, I.J.J., Wong, W.S.F., and Engelward, B.P. (2016). House dust mite–induced asthma causes oxidative damage and DNA double-strand breaks in the lungs. J. Allergy Clin. Immunol. *138*, 84–96.e1. https://doi.org/10.1016/j.jaci.2016.02.017.

40. Wang, Y., Lin, J., Shu, J., Li, H., and Ren, Z. (2018). Oxidative damage and DNA damage in lungs of an ovalbumin-induced asthmatic murine model. J. Thorac. Dis. *10*, 4819–4830. https://doi.org/10.21037/jtd.2018.07.74.

41. Ba, X., Aguilera-Aguirre, L., Sur, S., and Boldogh, I. (2015). 8-Oxoguanine DNA glycosylase-1-driven DNA base excision repair: role in asthma pathogenesis. Curr.Opin.Allergy Clin.Immunol. *15*, 89–97. https://doi.org/10.1097/ACI.0000000000000135.

42. Kau, A.L., Planer, J.D., Liu, J., Rao, S., Yatsunenko, T., Trehan, I., Manary, M.J., Liu, T.C., Stappenbeck, T.S., Maleta, K.M., et al. (2015). Functional characterization of IgA-targeted bacterial taxa from undernourished Malawian children that produce diet-dependent enteropathy. Sci. Transl. Med. *7*, 276ra24. https://doi.org/10.1126/scitranslmed.aaa4877.

43. Obiso, R.J., Lyerly, D.M., Van Tassell, R.L., and Wilkins, T.D. (1995). Proteolytic activity of the Bacteroides fragilis enterotoxin causes fluid secretion and intestinal damage in vivo. Infect. Immun. *63*, 3820–3826. https://doi.org/10.1128/iai.63.10.3820-3826.1995.

44. Obiso, R.J., Azghani, A.O., and Wilkins, T.D. (1997). The Bacteroides fragilis toxin fragilysin disrupts the paracellular barrier of epithelial cells. Infect. Immun. *65*, 1431–1439. https://doi.org/10.1128/iai.65.4.1431-1439.1997.

45. Wu, S., Lim, K.C., Huang, J., Saidi, R.F., and Sears, C.L. (1998). Bacteroides fragilis enterotoxin cleaves the zonula adherens protein, E-cadherin. Proc. Natl. Acad. Sci. USA *95*, 14979–14984. https://doi.org/10.1073/pnas.95.25.14979.

46. Cani, P.D., Bibiloni, R., Knauf, C., Waget, A., Neyrinck, A.M., Delzenne, N.M., and Burcelin, R. (2008). Changes in gut microbiota control metabolic endotoxemia-induced inflammation in high-fat diet-induced obesity and diabetes in mice. Diabetes *57*, 1470–1481. https://doi.org/10.2337/db07-1403.

47. Ueda, J., Starr, M.E., Takahashi, H., Du, J., Chang, L.Y., Crapo, J.D., Evers, B.M., and Saito, H. (2008). Decreased pulmonary extracellular superoxide dismutase during systemic inflammation. Free Radic. Biol. Med. *45*, 897–904. https://doi.org/10.1016/j.freeradbiomed.2008.06.016.

48. Cerdeño-Tárraga, A.M., Patrick, S., Crossman, L.C., Blakely, G., Abratt, V., Lennard, N., Poxton, I., Duerden, B., Harris, B., Quail, M.A., et al. (2005). Extensive DNA inversions in the B. fragilis genome control variable gene expression. Science *307*, 1463–1465. https://doi.org/10.1126/science.1107008.

49. Gueders, M.M., Paulissen, G., Crahay, C., Quesada-Calvo, F., Hacha, J., Van Hove, C., Tournoy, K., Louis, R., Foidart, J.M., Noël, A., and Cataldo, D.D. (2009). Mouse models of asthma: a comparison between C57BL/6 and BALB/c strains regarding bronchial responsiveness, inflammation, and cytokine production. Inflamm. Res. *58*, 845–854. https://doi.org/10.1007/S00011-009-0054-2.

50. Fang, L., Zhou, F., Wu, F., Yan, Y., He, Z., Yuan, X., Zhang, X., Zhang, T., and Yu, D. (2021). A mouse allergic asthma model induced by shrimp tropomyosin. Int. Immunopharmacol. *91*, 107289. https://doi.org/10.1016/J.INTIMP.2020.107289.

51. Kato, N., Liu, C., Kato, H., Watanabe, K., Nakamura, H., Iwai, N., and Ueno, K. (1999). Prevalence of enterotoxigenic Bacteroides fragilis in children with diarrhea in Japan. J. Clin. Microbiol. *37*, 801–803. https://doi.org/10.1128/jcm.37.3.801-803.1999.

52. Merino, V.R.C., Nakano, V., Liu, C., Song, Y., Finegold, S.M., and Avila-Campos, M.J. (2011). Quantitative detection of enterotoxigenic Bacteroides fragilis subtypes isolated from children with and without diarrhea. J. Clin. Microbiol. *49*, 416–418. https://doi.org/10.1128/JCM.01556-10.

53. Wagner, V.E., Dey, N., Guruge, J., Hsiao, A., Ahern, P.P., Semenkovich, N.P., Blanton, L.V., Cheng, J., Griffin, N., Stappenbeck, T.S., et al. (2016). Effects of a gut pathobiont in a gnotobiotic mouse model of childhood undernutrition. Sci. Transl. Med. *8*, 366ra164. https://doi.org/10.1126/scitranslmed.aah4669.

54. Schatz, M., Sorkness, C.A., Li, J.T., Marcus, P., Murray, J.J., Nathan, R.A., Kosinski, M., Pendergraft, T.B., and Jhingran, P. (2006). Asthma Control Test: reliability, validity, and responsiveness in patients not previously followed by asthma specialists. J. Allergy Clin. Immunol. *117*, 549–556. https://doi.org/10.1016/j.jaci.2006.01.011.

55. Zou, X.L., Wu, J.J., Ye, H.X., Feng, D.Y., Meng, P., Yang, H.L., Wu, W.B., Li, H.T., He, Z., and Zhang, T.T. (2021). Associations between gut microbiota and asthma endotypes: a cross-sectional study in South China based on patients with newly diagnosed asthma. J. Asthma Allergy *14*, 981–992. https://doi.org/10.2147/JAA.S320088.

56. Trivedi, M., and Denton, E. (2019). Asthma in children and adults—what are the differences and what can they tell us about asthma? Front. Pediatr. *7*, 256. https://doi.org/10.3389/fped.2019.00256.

57. Fuseini, H., and Newcomb, D.C. (2017). Mechanisms driving gender differences in asthma. Curr.Allergy Asthma Rep. *17*, 19. https://doi.org/10.1007/s11882-017-0686-1.

58. Polosa, R., and Thomson, N.C. (2013). Smoking and asthma: dangerous liaisons. Eur. Respir. J. *41*, 716–726. https://doi.org/10.1183/09031936.00073312.

59. Howard, E., Orhurhu, V., Huang, L., Guthrie, B., and Phipatanakul, W. (2019). The impact of ambient environmental exposures to microbial products on asthma outcomes from birth to childhood. Curr.Allergy Asthma Rep. *19*, 59. https://doi.org/10.1007/s11882-019-0890-2.

60. Chung, H., Pamp, S.J., Hill, J.A., Surana, N.K., Edelman, S.M., Troy, E.B., Reading, N.C., Villablanca, E.J., Wang, S., Mora, J.R., et al. (2012). Gut immune maturation depends on colonization with a host-specific microbiota. Cell *149*, 1578–1593. https://doi.org/10.1016/j.cell.2012.04.037.

61. Vujkovic-Cvijin, I., Sklar, J., Jiang, L., Natarajan, L., Knight, R., and Belkaid, Y. (2020). Host variables confound gut microbiota studies of human disease. Nature *587*, 448–454. https://doi.org/10.1038/s41586-020-2881-9.

62. Costello, E.K., Lauber, C.L., Hamady, M., Fierer, N., Gordon, J.I., and Knight, R. (2009). Bacterial community variation in human body habitats across space and time. Science *326*, 1694–1697. https://doi.org/10.1126/science.1177486.

63. Rothschild, D., Weissbrod, O., Barkan, E., Kurilshikov, A., Korem, T., Zeevi, D., Costea, P.I., Godneva, A., Kalka, I.N., Bar, N., et al. (2018). Environment dominates over host genetics in shaping human gut microbiota. Nature *555*, 210–215. https://doi.org/10.1038/nature25973.

64. Lozupone, C.A., Stombaugh, J.I., Gordon, J.I., Jansson, J.K., and Knight, R. (2012). Diversity, stability and resilience of the human gut microbiota. Nature *489*, 220–230. https://doi.org/10.1038/nature11550.

65. Alnahas, S., Hagner, S., Raifer, H., Kilic, A., Gasteiger, G., Mutters, R., Hellhund, A., Prinz, I., Pinkenburg, O., Visekruna, A., et al. (2017). IL-17 and TNF-α are key mediators of Moraxella catarrhalis triggered exacerbation of allergic airway inflammation. Front. Immunol. *8*, 1562–1611. https://doi.org/10.3389/fimmu.2017.01562.

66. Cho, R.L., Yang, C.C., Lee, I.T., Lin, C.C., Chi, P.L., Hsiao, L.D., and Yang, C.M. (2016). Lipopolysaccharide induces ICAM-1 expression via a c-Src/NADPH oxidase/ROS-dependent NF-κB pathway in human pulmonary alveolar epithelial cells. Am. J. Physiol. Lung Cell Mol. Physiol. *310*, L639–L657. https://doi.org/10.1152/AJPLUNG.00109.2014.

67. Goodwin, A.C., Destefano Shields, C.E., Wu, S., Huso, D.L., Wu, X., Murray-Stewart, T.R., Hacker-Prietz, A., Rabizadeh, S., Woster,

P.M., Sears, C.L., and Casero, R.A., Jr. (2011). Polyamine catabolism contributes to enterotoxigenic Bacteroides fragilis-induced colon tumorigenesis. Proc. Natl. Acad. Sci. USA *108*, 15354–15359. https://doi.org/10.1073/pnas.1010203108.

68. Hwang, S., Lee, C.G., Jo, M., Park, C.O., Gwon, S.Y., Hwang, S., Yi, H.C., Lee, S.Y., Eom, Y.B., Karim, B., and Rhee, K.J. (2020). Enterotoxigenic bacteroides fragilis infection exacerbates tumorigenesis in AOM/DSS mouse model. Int. J. Med. Sci. *17*, 145–152. https://doi.org/10.7150/ijms.38371.

69. Benard, A., Desreumeaux, P., Huglo, D., Hoorelbeke, A., Tonnel, A.B., and Wallaert, B. (1996). Increased intestinal permeability in bronchial asthma. J. Allergy Clin. Immunol. *97*, 1173–1178. https://doi.org/10.1016/S0091-6749(96)70181-1.

70. Hijazi, Z., Molla, A.M., Al-Habashi, H., Muawad, W.M., Molla, A.M., and Sharma, P.N. (2004). Intestinal permeability is increased in bronchial asthma. Arch. Dis. Child. *89*, 227–229. https://doi.org/10.1136/adc.2003.027680.

71. Caffarelli, C., Deriu, F.M., Terzi, V., Perrone, F., Dè Angelis, G., and Atherton, D.J. (2000). Gastrointestinal symptoms in patients with asthma. Arch. Dis. Child. *82*, 131–135. https://doi.org/10.1136/adc.82.2.131.

72. Jesenak, M., Zelieskova, M., and Babusikova, E. (2017). Oxidative stress and bronchial asthma in children-causes or consequences? Front. Pediatr. *5*, 162. https://doi.org/10.3389/fped.2017.00162.

73. Akiki, Z., Andrianjafimasy, M., Zerimech, F., Le Moual, N., Siroux, V., Dumas, O., Matran, R., and Nadif, R. (2019). High level of fluorescent oxidation products and worsening of asthma control over time. Respir.Res. *20*, 203. https://doi.org/10.1186/s12931-019-1173-0.

74. Tajik, N., Frech, M., Schulz, O., Schälter, F., Lucas, S., Azizov, V., Dürholz, K., Steffen, F., Omata, Y., Rings, A., et al. (2020). Targeting zonulin and intestinal epithelial barrier function to prevent onset of arthritis. Nat. Commun. *11*, 1995. https://doi.org/10.1038/s41467-020-15831-7.

75. Cardoso-Silva, D., Delbue, D., Itzlinger, A., Moerkens, R., Withoff, S., Branchi, F., and Schumann, M. (2019). Intestinal barrier function in gluten-related disorders. Nutrients *11*, 2325. https://doi.org/10.3390/nu11102325.

76. Oksanen, J., Simpson, G., Blanchet, F., Kindt, R., Legendre, P., Minchin, P., et al. (2023). vegan: Community Ecology Package. R package version 2.6-5, https://github.com/vegandevs/vegan.

77. McMurdie, P.J., and Holmes, S. (2013). phyloseq: An R Package for Reproducible Interactive Analysis and Graphics of Microbiome Census Data. PLoS One *8*, e61217. https://doi.org/10.1371/JOURNAL.PONE.0061217.

78. Love, M.I., Huber, W., and Anders, S. (2014). Moderated estimation of fold change and dispersion for RNA-seq data with DESeq2. Genome Biol. *15*, 550–621. https://doi.org/10.1186/s13059-014-0550-8.

79. Griffith, D.M., Veech, J.A., and Marsh, C.J. (2016). Cooccur: probabilistic species co-occurrence analysis in R. J. Stat. Softw. *69*, 1–17. https://doi.org/10.18637/jss.v069.c02.

80. Bushnell, B. BBMap. https://sourceforge.net/projects/bbmap/.

81. Bankevich, A., Nurk, S., Antipov, D., Gurevich, A.A., Dvorkin, M., Kulikov, A.S., Lesin, V.M., Nikolenko, S.I., Pham, S., Prjibelski, A.D., et al. (2012). SPAdes: a new genome assembly algorithm and its applications to single-cell sequencing. J. Comput. Biol. *19*, 455–477. https://doi.org/10.1089/cmb.2012.0021.

82. Seemann, T. (2014). Prokka: rapid prokaryotic genome annotation. Bioinformatics *30*, 2068–2069. https://doi.org/10.1093/bioinformatics/btu153.

83. Kuperman, D.A., Lewis, C.C., Woodruff, P.G., Rodriguez, M.W., Yang, Y.H., Dolganov, G.M., Fahy, J.V., and Erle, D.J. (2005). Dissecting asthma using focused transgenic modeling and functional genomics. J. Allergy Clin. Immunol. *116*, 305–311. https://doi.org/10.1016/j.jaci.2005.03.024.

84. Caporaso, J.G., Lauber, C.L., Walters, W.A., Berg-Lyons, D., Lozupone, C.A., Turnbaugh, P.J., Fierer, N., Knight, R., Berg-Lyons, D., Lozupone, C.A., et al. (2011). Global patterns of 16S rRNA diversity at a depth of millions of sequences per sample. Proc. Natl. Acad. Sci. USA *108*, 4516–4522. https://doi.org/10.1073/pnas.1000080107.

85. Wang, Q., Garrity, G.M., Tiedje, J.M., and Cole, J.R. (2007). Naïve Bayesian classifier for rapid assignment of rRNA sequences into the new bacterial taxonomy. Appl. Environ. Microbiol. *73*, 5261–5267. https://doi.org/10.1128/AEM.00062-07.

86. McMurdie, P.J., and Holmes, S. (2014). Waste not, want not: why rarefying microbiome data is inadmissible. PLoS Comput. Biol. *10*, e1003531. https://doi.org/10.1371/journal.pcbi.1003531.

87. Nearing, J.T., Douglas, G.M., Hayes, M.G., MacDonald, J., Desai, D.K., Allward, N., Jones, C.M.A., Wright, R.J., Dhanani, A.S., Comeau, A.M., and Langille, M.G.I. (2022). Microbiome differential abundance methods produce different results across 38 datasets. Nat. Commun. *13*, 342–416. https://doi.org/10.1038/s41467-022-28034-z.

88. Planer, J.D., Peng, Y., Kau, A.L., Blanton, L.V., Ndao, I.M., Tarr, P.I., Warner, B.B., and Gordon, J.I. (2016). Development of the gut microbiota and mucosal IgA responses in twins and gnotobiotic mice. Nature *534*, 263–266. https://doi.org/10.1038/nature17940.

89. Baym, M., Kryazhimskiy, S., Lieberman, T.D., Chung, H., Desai, M.M., and Kishony, R. (2015). Inexpensive multiplexed library preparation for megabase-sized genomes. PLoS One *10*, 01280366–e128115. https://doi.org/10.1371/journal.pone.0128036.

90. Yoon, S.H., Ha, S.M., Lim, J., Kwon, S., and Chun, J. (2017). A large-scale evaluation of algorithms to calculate average nucleotide identity. Antonie Leeuwenhoek *110*, 1281–1286. https://doi.org/10.1007/s10482-017-0844-4.

91. Patnode, M.L., Bando, J.K., Krummel, M.F., Locksley, R.M., and Rosen, S.D. (2014). Leukotriene B4 amplifies eosinophil accumulation in response to nematodes. J. Exp. Med. *211*, 1281–1288. https://doi.org/10.1084/jem.20132336.

92. Langmead, B., and Salzberg, S.L. (2012). Fast gapped-read alignment with Bowtie 2. Nat. Methods *9*, 357–359. https://doi.org/10.1038/nmeth.1923.

93. Anders, S., Pyl, P.T., and Huber, W. (2015). HTSeq-A Python framework to work with high-throughput sequencing data. Bioinformatics *31*, 166–169. https://doi.org/10.1093/bioinformatics/btu638.

94. Korotkevich, G., Sukhov, V., Budin, N., Shpak, B., Artyomov, M., and Sergushichev, A. (2016). Fast gene set enrichment analysis. Preprint at bioRxiv, 060012. https://doi.org/10.1101/060012.

95. Thevaranjan, N., Puchta, A., Schulz, C., Naidoo, A., Szamosi, J.C., Verschoor, C.P., Loukov, D., Schenck, L.P., Jury, J., Foley, K.P., et al. (2017). Age-associated microbial dysbiosis promotes intestinal permeability, systemic inflammation, and macrophage dysfunction. Cell Host Microbe *21*, 455–466.e4. https://doi.org/10.1016/j.chom.2017.03.002.

96. Knoop, K.A., Gustafsson, J.K., McDonald, K.G., Kulkarni, D.H., Coughlin, P.E., McCrate, S., Kim, D., Hsieh, C.S., Hogan, S.P., Elson, C.O., et al. (2017). Microbial antigen encounter during a preweaning interval is critical for tolerance to gut bacteria. Sci. Immunol. *2*, eaao1314. https://doi.org/10.1126/sciimmunol.aao1314.

97. Breiman, L. (2001). Random forests. Mach. Learn. *45*, 5–32. https://doi.org/10.1023/A:1010933404324.

98. Hu, Y., Feng, Y., Wu, J., Liu, F., Zhang, Z., Hao, Y., Liang, S., Li, B., Li, J., Lv, N., et al. (2019). The gut microbiome signatures discriminate healthy from pulmonary tuberculosis patients. Front. Cell. Infect. Microbiol. *9*, 90–98. https://doi.org/10.3389/fcimb.2019.00090.

STAR★METHODS

KEY RESOURCES TABLE

REAGENT or RESOURCE	SOURCE	IDENTIFIER
Antibodies		
PE anti-mouse SiglecF (Clone E50-2240)	BD Pharmigen™	Cat# 562068; RRID: AB_10896143
FITC anti-mouse CD4 (Clone GK1.5)	Biolegend	Cat# 100406; RRID: AB_312691
FITC anti-mouse CD11c (Clone N418)	Biolegend	Cat# 117306; RRID: AB_313775
PE anti-mouse CD44 (Clone IM7)	BD Pharmigen™	Cat# 553134; RRID: AB_394649
PE anti-mouse IL-17A (Clone TC11-18H0.1)	Biolegend	Cat# 506904; RRID: AB_315464
PerCP-Cy™5.5 anti-mouse TCR β chain (Clone H57-597)	BD Pharmigen™	Cat# 560657; RRID: AB_1727575
PE-Cy™7 anti-mouse CD11b (Clone M1/70)	BD Pharmigen™	Cat# 552850; RRID: AB_394491
PE/Cyanine7 anti-mouse CD62L (Clone MEL-14)	Biolegend	Cat# 104418; RRID: AB_313103
APC anti-mouse Ly6G (Clone 1A8)	Biolegend	Cat# 127613; RRID: AB_1877163
APC anti-mouse CD45 (Clone 30-F11)	Biolegend	Cat# 103112; RRID: AB_312977
PerCP anti-mouse CD45 (Clone 30-F11)	Biolegend	Cat# 103129; RRID: AB_893343
APC/Cyanine7 anti-mouse I-A/I-E (Clone M5/114.15.2)	Biolegend	Cat# 107627; RRID: AB_1659252
eFluor450 anti-mouse FoxP3 (Clone FJK-16s)	eBioscience™	Cat# 48-5773-82; RRID: AB_1518812
eFluor450 anti-mouse IL-13 (Clone 13A)	eBioscience™	Cat# 48-7133-80; RRID: AB_11219690
Brilliant Violet 421™ anti-mouse F4/80 (Clone BM8)	Biolegend	Cat# 123131; RRID: AB_10901171
APC/Cyanine7 anti-mouse TCR β chain (Clone H57-597)	Biolegend	Cat# 109220; RRID: AB_893624
PE/Cyanine7 anti-mouse IFNγ (Clone XMG1.2)	Biolegend	Cat# 505825; RRID: AB_1595591
APC anti-mouse TNFα (Clone MP6-XT22)	BD Pharmigen™	Cat# 561062; RRID: AB_2034022
Bacterial and virus strains		
Bacteroides fragilis (BFM04319)	Isolated from stool of a human subject with asthma in this study by plating stool anaerobically on brain-heart-infusion media supplemented to 0.1% porcine mucin.	NA
Bacteroides fragilis (VPI2553)	Received as a gift from the laboratory of Jeffrey I. Gordon. Can be acquired from ATCC.	Cat# 25285
Biological samples		
Human stool samples were obtained from both an adult (ages 18-40 years) and a pediatric population (ages 6-10 years).	The study cohorts came from the Microbiome in Asthma Research Study (MARS)	NA
Chemicals, peptides, and recombinant proteins		
Fetal Bovine Serum	Thermo Fisher Scientific (GIBCO™)	Cat# 26140-079
BD Difco™ Bacto™ Brain Heart Infusion	Fisher Scientific	Cat# DF0037-07-0
Mucin from porcine stomach	Millipore Sigma	Cat# M1778
L-Cysteine hydrochloride anhydrous	Millipore Sigma	Cat# C1276
BD Difco™ Dehydrated Culture Media: Noble Agar	Fisher Scientific	Cat# DF0142-17-0
DL-Histidine monohydrochloride monohydrate	Millipore Sigma	Cat# H7875
Hematin porcine	Millipore Sigma	Cat# H3281
Resazurin sodium salt	Millipore Sigma	Cat# R7017
Albumin from chicken egg white	Millipore Sigma	Cat# A5503

(*Continued on next page*)

Continued

REAGENT or RESOURCE	SOURCE	IDENTIFIER
Imject™ Alum Adjuvant	Thermofisher Scientific	Cat# 77161
Phenol/Chloroform/Isoamyl Alcohol (25:24:1 Mixture, pH 6.7/8.0, Liq.)	Fisher Scientific	Cat# BP1752I-400
BioSpec Products 0.1 MM Zirconia/Silica Beads	Fisher Scientific	Cat# NC0362415
Low Carbon Steel Balls (5/32'')	McMaster-Carr	Cat# 96455K73
AMPure XP Reagent, 5 mL	Beckman Coulter	Cat# A63880
HEPES (Fine White Crystals/Molecular Biology), Fisher BioReagents™	Fisher Scientific	Cat# BP310-500
Liberase™ DL Research Grade	Millipore Sigma (Roche)	Cat# 5466202001
DNase I	Millipore Sigma (Roche)	Cat# 10104159001
ACK Lysing Buffer	Thermofisher (Gibco)	Cat# A1049201
PMA	Sigma-Aldrich	Cat# P1585
Ionomycin from *Streptomyces conglobatus*	Sigma-Aldrich	Cat# I9657
eBioscience™ Monensin Solution (1000X)	Thermofisher (Invitrogen)	Cat# 00-4505-51
eBioscience™ Brefeldin A Solution (1000X)	Thermofisher (Invitrogen)	Cat# 00-4506-51
RNA*later*™ Stabilization Solution	Thermofisher (Invitrogen)	Cat# AM7021
TRIzol™ Reagent	Thermofisher (Invitrogen)	Cat# 15596018
Fluorescein isothiocyanate–dextran	Millipore Sigma (Sigma-Aldrich)	Cat# 46944
Thomas Scientific GelRed Nucleic Acid Gel Stain, 10,000X in Water, 0.1mL	Fisher Scientific (Thomas Scientific)	Cat# NC9938951
Critical commercial assays		
Illumina DNA Prep (Nextera)	Illumina	Cat# FC-121-1030
Bacteria Counting Kit, for flow cytometry (SYTO-BC)	Thermofisher (Invitrogen)	Cat# B7277
QIAquick 96 PCR Purification Kit	Qiagen	Cat# 28183
Quant-iT™ dsDNA Assay Kits, broad range (BR)	Thermofisher (Invitrogen)	Cat# Q33130
RNAeasy Mini Kit	Qiagen	Cat# 74104
Quant-it™ RiboGreen RNA Assay Kit and RiboGreen RNA Reagent, RediPlate™ 96 RiboGreen™ RNA Quantitation Kit	Thermofisher (Invitrogen)	Cat# R11490
NEBNext® Ultra™ II DNA Library Prep Kit for Illumina®	Illumina	Cat# E7645L
Power SYBR™ Green PCR Master Mix	Thermofisher (Applied Biosystems)	Cat# 4367659
LEGENDplex™ Mouse Inflammation Panel (13-plex) with V-bottom Plate	Biolegend	Cat# 740446
DNeasy Blood & Tissue Kit (50)	Qiagen	Cat# 69504
DNA/RNA Oxidative Damage (High Sensitivity) ELISA Kit	Cayman Chemicals	Cat# 589320
BD Microtainer™ Capillary Blood Collector and BD Microgard™ Closure	Fisher Scientific (BD)	Cat# 02-675-185
Epredia™ Shandon™ Kwik-Diff™ Stains	Fisher Scientific (Epredia)	Cat# 99-907-01
AllPrep PowerFecal DNA/RNA Kit	Qiagen	Cat# 80244
cDNA Synthesis: EasyScript Plus™ cDNA Synthesis Kit	Lambda Biotech	Cat# G236
Calprotectin ELISA Assay Kit	Eagle Biosciences	Cat# CAL35-K01

(*Continued on next page*)

Continued

REAGENT or RESOURCE	SOURCE	IDENTIFIER
Deposited data		
Sequencing Data	This paper	European Nucleotide Archive Accesion Number: PRJEB45298
Experimental models: Organisms/strains		
Mouse: Germ-free C57BL/6J: WT C57BL/6J	Bred in house	N/A
Oligonucleotides		
See Table S8 for a list of oligonucleotides	N/A	N/A
Software and algorithms		
R version 4.2.1 or higher	R Development Core Team, 2011	https://www.r-project.org/
FlowJo v10	BD	RRID: SCR_008520, https://www.flowjo.com/solutions/flowjo/downloads
BD FACSDiva™ software	BD Bioscience	RRID: SCR_001456
DADA2 (version 1.10.1 in R)	Callahan et al., 2016[28]	https://benjjneb.github.io/dada2/
vegan (version 2.5.7 in R)	Oksanen et al., 2023[76]	https://github.com/vegandevs/vegan
phyloseq (version 1.28.0 in R)	McMurdie and Holmes, 2013[77]	https://joey711.github.io/phyloseq/
DESEQ2 (version 1.24.0 in R)	Love et al., 2014[78]	https://bioconductor.org/packages/release/bioc/html/DESeq2.html
cooccur (version 1.3 in R)	Griffith et al., 2016[79]	https://rdrr.io/cran/cooccur/man/cooccur.html
Bbtools	Bushnell et al. 2017[80]	sourceforge.net/projects/bbmap/
SPAdes version 3.11.0	Bankevich et al., 2012[81]	https://cab.spbu.ru/software/spades/
prokka (version 1.14.6)	Seemann, T. 2014[82]	https://github.com/tseemann/prokka
gnominator (version 1.0 in R)	This paper	Zenodo: https://doi.org/10.5281/zenodo.7522060

RESOURCE AVAILABILITY

Lead contact

Further information and requests for resources should be directed to and will be fulfilled by the lead contact, Andrew Kau (akau@wustl.edu).

Materials availability

All unique/stable reagents generated in the study are available from the lead contact with a completed materials transfer agreement.

Data and code availability

- RNASeq and V4 16S rRNA and genome sequencing data have been deposited at the European Nucleotide Archive (https://www.ebi.ac.uk/ena/browser/home) and are publicly available as of the date of publication under project accession number PRJEB45298.
- All original code to run the mixture distribution-based NBC is available via Zenodo (https://doi.org/10.5281/zenodo.7522060).
- Any additional information required to reanalyze the data reported in this paper is available from the lead contact upon request.

EXPERIMENTAL MODEL AND SUBJECT DETAILS

Human subjects

The Microbiome and Asthma Research Study (MARS) was designed to investigate the role of intra- and interpersonal variation in the gut microbiome on human asthma pathogenesis. This cohort has been described in a previous manuscript.[27] Briefly, all individuals were either healthy or had moderate-to-severe

asthma and had not received oral corticosteroids or antibiotics in the 30 days prior to enrollment. Individuals were included in the asthma cohort if they had at least one positive skin prick test or serum aeroallergen-specific IgE. Two age cohorts were recruited representing a pediatric (aged 6-10 years) and an adult (aged 18-40 years) population. Of 104 patients initially enrolled in the study, 103 were asked to provide samples and fill out the questionnaire. Of the 103 asked, 6 were excluded due to insufficient medical documentation and 2 did not provide stool samples (Figure S1A). As summarized in Table S1A, a total of 95 patients provided stool and relevant demographic data, including antibiotic and asthma medication use over the past year, and were ultimately included in this study. Fecal collection tubes with spoons and toilet hats were provided to patients after enrollment. Patients either provided a fecal specimen at the recruitment visit or collected and stored a fecal sample at home at -20°C for no more than 24 hours before returning the sample to the study site where it was stored at -80°C until processing.

MARS was approved by the Washington University Institutional Review Board (IRB ID# 201412035). Written informed consent documents were obtained from all MARS subjects or their legal guardians. All animal studies conformed to ethics of animal experimentation and were approved by the Institutional Animal Care and Use Committee (IACUC Protocol ID #: 20180286 and 21-0394).

Experimental animals and ethics

Germ-free C57BL/6 mice were bred and maintained in sterile flexible vinyl isolators. Sterility was assured by monthly monitoring of mouse stools by 16S rRNA gene PCR amplification as well as aerobic and anaerobic culture. Germ-free mice were maintained on a strict 12 hour light cycle and a diet of autoclaved mouse chow (LabDiet: Standard Diet 5021 - Autoclavable Mouse Breeder). For each experiment no more than five mice were housed in a cage. Mice were randomly assigned to experimental groups, with the exception of age and gender matching mice in each experimental group. Investigators were not blinded to experimental groups. Male and female mice within a group were caged separately but housed and handled within the same flexible vinyl isolator. Within all experiments, mice of the same sex and receiving the same human microbiota (or isolate) were caged together. Sex was tested, but not a significant contributor to the phenotypes described unless otherwise shown.

Isolation and growth *Bacteroides fragilis* strains

B. fragilis strain BFM04319 was isolated from MARS0043 (subject with asthma) stool using anaerobic culture methods. Briefly, a 10 mg/mL stock of homogenized stool in 10% glycerol/PBS was thawed in a Coy anaerobic chamber, plated on BHI/mucin agar containing 0.1% mucin, 0.1% Resazurin, and 0.05% L-Cysteine (HCl) and 1.2 mg/L histidine/hematin and incubated at 37°C for 6 days. Single colonies were isolated in BHI/mucin liquid media and stocked in 10% glycerol. Culture purity and identity was confirmed by V4 16S sequencing. Non-toxigenic *B. fragilis* VPI2553 was provided as a generous gift from Dr. Jeffrey I. Gordon. All strains were grown anaerobically in BHI/mucin media as above at 37°C for 24 hours before diluting 1:2 with 20% glycerol, freezing, and gavaging into GF mice.

METHOD DETAILS

Humanized gnotobiotic mouse model

We began with frozen pulverized fecal samples brought into an anaerobic chamber and transferred into reduced 1X PBS supplemented with 0.1% Resazurin and 0.05% L-Cysteine (HCl) to a concentration of 10 mg/mL. Fecal samples were then thoroughly homogenized using a sterilized probe homogenizer. Resuspended fecal samples were diluted 1:2 in 20% glycerol in PBS/Cysteine and stored in sealed HPLC vials at -80°C until use. Sample viability was confirmed by outgrowth of 100 uL of prepped gavage material on BHI/mucin agar containing 0.1% mucin, 0.1% Resazurin, and 0.05% L-Cysteine (HCl) and 1.2 mg/L histidine/hematin. A minimum of $1x10^4$ CFU/mg was used for colonization. Germ-free mice were humanized by oral gavage of 200 mL of a thawed homogenized stool sample. The microbiota was allowed to stabilize over two to four weeks prior tofurther intervention. All experiments were performed with at least one asthmatic and one healthy microbiota and separate donor groups were maintained in separate isolators to prevent cross-contamination. For the additional humanization experiments seen in Figure 6, we selected asthmatic microbiota containing ETBF, of which 5 were viable in culture outgrowth. For each donor with asthma, we selected a healthy sample within the same age group – either adult or pediatric – that did not contain ETBF but had the highest pairwise feature score (Figure S7C). We assessed the quality of human microbiota transplantation by calculating the Bray-Curtis dissimilarity of 16S rRNA sequencing data between human

donors and murine recipients. We then ranked the average dissimilarity between recipients and donor and only included recipient groups who were the top ranked in similarity to their human donor.

Allergic airway inflammation model

Allergic airway inflammation was induced in mice using chicken egg ovalbumin as previously described.[27,83] The ovalbumin model of sensitization and challenge is convenient for gnotobiotic experiments since it is a pure, sterile protein and has previously been used in other gnotobiotic systems.[10] Germfree mice were sensitized on days 0, 7, and 14 by intraperitoneal injections of 200 mL of OVA/alum: ovalbumin (50 mg, Sigma grade V) combined with Imject Alum (Thermo Scientific) as per the manufacturer's recommendations. Mice were challenged on days 20 - 22 by intranasal introduction of 1 mg ovalbumin suspended in 50 mL sterile PBS while under anesthesia. Ovalbumin lot numberSLBK645SV was used for experiments shown in Figures 3, 4, and 5. Ovalbumin lot numberSLBQ9036V was used for experiments shown in Figure 6. We controlled for this by only directly comparing experimental groups of mice treated with the same lot of ovalbumin. Control mice were neither sensitized nor challenged unless otherwise noted.

Processing of stool and 16S rRNA profiling library preparation

Human stool was pulverized in a biosafety cabinet with liquid nitrogen using a pestle and mortar and aliquoted into 50 - 100 mg samples and stored at -80°C prior to use. For both human and mouse fecal specimens, crude DNA was extracted using phenol:chloroform:isoamyl alcohol and homogenized with a bead beater using sterilized zirconium and steel beads as previously described.[42] The aqueous layer was then purified with a 96-well QIAGEN PCR Clean up kit and quantitated by measuring the absorbance at 260/280 nm. DNA concentrations were normalized to 5 ng/mL using a broad range Quant-iT™ dsDNA Assay and 10 ng of DNA was used to PCR amplify the V4 16S rRNA region using barcoded primers as previously described.[84] PCR-amplified DNA was pooled to equal concentration and the library purified using AMPure XP SPRI beads. DNA was sequenced using a MiSeq with 2x250 bp chemistry. All samples had a minimum read-depth of 5000.

ANALYSIS OF 16S RRNA DATA

Fastq files were demultiplexed and binned into amplicon sequence variants (ASVs; Table S6) using DADA2 as previously described.[27] Taxonomic determination of ASV sequences to the lowest possible level was performed with RDP Classifier[85] using a database built to permit species level identification[42] with a minimum bootstrap support of 80%.

ASVs were normalized using total sum scaling. Diversity analysis of 16S data was carried out with vegan (v2.5-7) and phyloseq (v1.28.0) in R. Richness was estimated as the average count of observed taxa after rarefying to 5000 reads using the vegan rarefy function. Sequential PERMANOVA was carried out for 100,000 iterations to achieve a minimum p-value of 10^{-5} using adonis2 in vegan. PERMDISP2 was performed with the betadisper function in vegan. Differential abundance analysis was carried out with DESEQ2 (version 1.24.0) as previously described.[78,86]Random permutation of samples revealed a DESEQ2 positivity rate of 6.7% for asthma and 6.8% for age, consistent with previous reports of DESEQ2 performing with a slightly higher than the expected 5% positivity rate, but less than the positivity rate of real data.[87] Batch effect in 16S data resulting from sequencing run differences was assessed using PERMANOVA and found to contribute significantly to the variance in the data, but did not otherwise affect our results (see Table S2). Co-occurrence was calculated using the cooccur package.[79]

IgA-seq

We performed IgA-seq on mouse fecal samples as previously described.[42] In brief, fecal samples were prepared in reduced PBS, stained with polyclonal goat anti-human IgA (Abcam #ab96998) or goat anti-mouse IgA (Abcam #ab97104) fluorescently labeled with DyLight649. Following antibody staining, samples were washed with PBS and resuspended in 100 mM HEPES and 150 mM NaCl containing a 1:4000 dilution of Syto-BC (Invitrogen). Samples were run and acquired on a BD Aria II maintained in a laminar flow biosafety cabinet. Input, IgA- and IgA+ positive fractions were acquired and sequenced as previously described.[88] To analyze these data we used a previously reported IgA index.[42]

Whole genome sequencing of BFM04319

Genomic DNA was extracted from *B. fragilis* strain BFM04319 by phenol/chloroform extraction. We then used an adaptation of the Nextera Library Prep kit (Illumina, cat. FC-121-1030/1031)[89] and sequenced on a MiSeq to achieve ~80X coverage of the 5Mbp ETBF genome. Reads were trimmed by quality and adapter content with bbtools (sourceforge.net/projects/bbmap/). Scaffolds were created with SPAdes[81] and annotated with prokka.[82] Our assembly had an N50 of 432688 and an L50 of 5. BFM04319 had an average nucleotide identity of 98.84% to the genome of the *B. fragilis* type strain VPI2553 (NCBI reference sequence: CR626927.1).[90]

Immune cell isolation from tissues

Cells were extracted from tissues as described.[27] Briefly, lungs were minced and incubated in digestion buffer (0.2 U/ml Liberase DL (Roche Applied Sciences) and 0.2 mg/ml DNase (Sigma) in Hank's Buffered salt Solution (without Ca^{2+}/Mg^{2+}) for 25 minat 37°C before being passed through a 70μm cell strainer.[91] Spleen and lymph nodes were dissociated manually and passed through a 70 μM cell strainer. Red blood cells were removed from lung and spleen samples by treatment with ACK lysis buffer.

Flow cytometry of isolated immune cells

Data were acquired on a FACSCanto II (BD Biosciences) equipped for the detection of eight fluorescent parameters. The following antibodies were used: PE anti-mouse SiglecF (Clone E50-2240; BD Pharmigen™), FITC anti-mouse CD4 (Clone GK1.5, Biolegend), FITC anti-mouse CD11c (Clone N418, Biolegend), PE anti-mouse CD44 (Clone IM7, BD Pharmigen™), PE anti-mouse IL-17A (Clone TC11-18H0.1, Biolegend), PerCP-Cy™5.5 anti-mouse TCR β chain (Clone H57-597, BD Pharmigen™), PE-Cy™7 anti-mouse CD11b (Clone M1/70, BD Pharmigen™), PE/Cyanine7 anti-mouse CD62L (Clone MEL-14, Biolegend), APC anti-mouse Ly6G (Clone 1A8, Biolegend), APC anti-mouse CD45 (Clone 30-F11, Biolegend), PerCP anti-mouse CD45 (Clone 30-F11, Biolegend), APC/Cyanine7 anti-mouse I-A/I-E (Clone M5/114.15.2, Biolegend), eFluor450 anti-mouse FoxP3 (Clone FJK-16s, eBioscience™), eFluor450 anti-mouse IL-13 (Clone 13A, eBioscience™), Brilliant Violet 421™ anti-mouse F4/80 (Clone BM8, Biolegend), APC/Cyanine7 anti-mouse TCR β chain (Clone H57-597, Biolegend), PE/Cyanine7 anti-mouse IFNγ (Clone XMG1.2, Biolegend), APC anti-mouse TNFα (Clone MP6-XT22, BD Pharmigen™). Intracellular staining of cytokines was conducted as previously described.[27] Briefly, cells were stimulated for 4 hat 37°C with PMA (10ng/mL), ionomycin (200ng/mL), monensin (1:1000), and brefeldin A (1:1000). LIVE/DEAD Fixable Aqua Dead Cell Stain Kit was used to assess cell viability in all panels. Data analysis was performed using FlowJo version 10 or higher software (Treestar, Ashland, OR). Gating strategies are summarized in Figures S5F–S5H.

Transcriptional profiling of mouse lungs

We isolated total RNA from mouse lungs and performed transcriptomic analysis as previously described.[27] Whole lungs were removed from mice and homogenized in 2 mL of TRIzol reagent. Crude RNA was extracted from 0.3 mLs of homogenized tissue using the QIAgen RNAeasy kit following manufacturer's protocol. Reads were mapped to the mouse genome using bowtie2 (v2.3.4.1),[92] quantified at the gene level using htseq (v 0.9.1),[93] and differentially expressed genes were identified using DESeq2 (v1.24.0).[78] Functional pathways altered during colonization and/or OSC were identified using gene set enrichment analysis FGSEA (fgsea R package; v1.10.1)[94] with KEGG and GO databases. PERMANOVA was performed using adonis (vegan R package; v2.5-7) and the post hoc test was performed with pairwise.adonis (pairwiseAdonis, v0.3).

Lung RT-qPCR

RNA from flash-frozen, pulverized lung tissue or lung tissue stored in RNALater (Invitrogen cat. AM7021) was extracted by probe homogenization in TRIzol Reagent followed by chloroform phase separation. DNase I (Qiagen) was then used to degrade DNA according to the manufacturer and this reaction was carried onto Qiagen's RNeasy Mini kit for purification of RNA. We then quantified the RNA with a Quanti-iT Ribogreen RNA Assay kit (Invitrogen cat. R11490) and synthesized cDNA with a high-capacity RNA-to-cDNA kit (AB cat. 4387406). RT-qPCR was performed on a Biorad CFX96 Real-Time System using Power SYBR Green PCR Master Mix (AB 4367659). Primer pairs used in this paper are shown in Table S8 including GAPDH as the reference gene. Samples were run in triplicate and were excluded if the range of raw Ct values for target or reference exceeded 2.

Protein quantification

Mouse Serum IgE specific to ovalbumin was quantified by sandwich ELISA.[27] Briefly, plates were coated with 10 mg/mL purified ovalbumin overnight at 4°C and then blocked with PBS 1x with 1% BSA. Sera were diluted 1:10 and plated alongside purified OVA-specific IgE (Clone 2C6, AbD Serotec) as a standard curve. The plate was incubated for 2 hours at room temperature. Bound IgE was detected using goat anti-mouse IgE-HRP (Clone RME-1, Biolegend). Serum IL-17A was measured as part of a LEGENDPlex Multiplex protein assay (Biolegend) following the manufacturer's protocol.

DNA/RNA oxidative damage ELISA

DNA was extracted from the lungs of mice by homogenization and ethanol precipitation or using the QIAGEN Dneasy Blood & Tissue Kit. To estimate pulmonary oxidative stress we measured oxidized guanosine (8- hydroxyguanosine, 8-hydroxy-2'-deoxyguanosine, and 8-hydroxyguanine) from extracted lung DNA by ELISA (Cayman Chemical cat. 589320) following the manufacturer's instructions and analysis template.

Intestinal permeability assay

In order to assess intestinal permeability, FITC-Dextran gut-to-serum absorption was measured at the time of sacrifice as previously described.[95,96] Briefly, a baseline blood sample (150 - 250 uL) was taken from each mouse via facial vein puncture. After one hour of fasting, the mice were orally gavaged with 200 mL of 40 mg/ml FITC-Dextran (4 kDa; Sigma Aldrich) in sterile PBS. Food and water were then withheld for an additional 45 minutes. After three hours mice were sacrificed and blood was collected by cardiac puncture. Serum was separated from blood samples using serum separator tubes according to manufacturer's instructions (BD microtainer). Fluorescence of pre- and post-gavage serum were measured (at a 5-fold dilution in PBS) using an excitation wavelength of 485nm and an emission wavelength of 528nm. A standard curve from 0 to 40 mg/ml FITC-Dextran read on the same plate was used to convert the RFU values to concentration of FITC-Dextran. Finally, pre-gavage serum FITC-Dextran concentrations were subtracted from post-gavage serum FITC-Dextran concentrations to quantify leakage from the gastrointestinal tract to the circulation.

Cytospin

Bronchoalveolar lavage was collected by flushing the mouse lungs using 1 mL of 0.1% bovine serum albumin (BSA) in sterile PBS. $5x10^5$ cells of each sample were loaded onto a slide using a Shandon Cytospin 2. Slides were then methanol fixed and stained with eosin and methylene blue following kit directions (ThermoScientific Shandon KwikDiff Stains). Cells were counted using a bright-field microscope at 400X magnification. 300 non-red blood cells were counted per sample, with careful scanning to ensure no repetition between high power fields.

Screening for bft in subject stool samples

Purified DNA from stool samples containing *Bacteroidesfragilis* based on V4-16S rRNA community profiling were normalized to 5 ng/mL. PCR was used to amplify the constant c-terminal region of the *bft* gene (Table S8).[51] The results of the reaction were assessed using a 2% agarose gel stained with GelRed (Biotium). Previous literature has identified this method suffers from low sensitivity, so we also conducted qPCR on the same samples.[52] qPCR primers were designed based on the *bft* sequence identified in BFM04319 and verified by confirming amplification against purified BFM04319 genome, and a complete fecal community harboring BFM04319 (AO stool gDNA), but not in a community lacking BFM04319 (HO stool gDNA). A single band of the expected size was detected by electrophoresis of BFM04319 genome amplification and AO stool gDNA amplification, but not HO stool gDNA. A dilution series of *B. fragilis* genome was used to demonstrate primers were sufficiently sensitive to detect *bft* from less than $2*10^{-5}$ ng of *B. fragilis* genome. The presence of a band or a Cq value of less than 35 was considered a positive result and indicated the presence of *bft* in patient stool.

Quantitation of bft expression in mouse cecal contents

Mouse cecal content RNA and DNA was extracted using the QIAgen AllPrep PowerFecal DNA/RNA kit as per kit instructions (cat. 80244). Nucleic acids were quantitated and cDNA synthesis was performed on 450 ng of cecal RNA using the Lambda Biotech EasyScriptPlus cDNA Synthesis kit (cat. G236) and a primer specific to *bft* (see Table S8). qPCR was performed as previously described. Copies of *B. fragilis* genome

were estimated by comparing cycle number against a dilution series of purified BFM04319 genome and then normalized to the amount of nucleic acid per milligram of cecal content.

Quantitation of calprotectin in human stool samples

Human fecal calprotectin was measured using the Calprotectin ELISA Assay Kit (Eagle Biosciences cat. CAL35-K01) following manufacturer's directions. Between 50 and 100 mg of pulverized human stool was used for each assayed sample.

QUANTIFICATION AND STATISTICAL ANALYSIS

Statistics

Statistics and analysis were all performed in R Version 3.6.3. Data are presented as mean with SEM. Statistical significance was conducted using an unpaired Wilcoxon test or Kruskal Wallis test with a post hoc Dunn test where appropriate. Adjustment of p-values for multiple hypotheses was performed using Benjamini-Hochberg correction. Boxplots display IQR and whiskers display 1.5*IQR. The following symbols were used to designate significance: *$p < 0.05$, **$p < 0.01$, ***$p < 0.001$.

Mixture distribution Naïve Bayes' classifier for 16S profiling of asthma vs. healthy patients

Input data

Raw ASV counts data were normalized to total counts (relative abundance). To be included in the NBC, a taxon had to appear in at least 7 samples. This number was determined by calculating how many samples are required to identify enrichment of a taxa in either the healthy or asthmatic cohort with 95% confidence, based on presence/absence alone (Binomial Test). In total, 392 ASVs between 95 human stool subjects were included in this analysis.

Algorithm

The algorithm is summarized in Figure S8B. By Bayes' theorem, the probability that a microbiome composed of many taxa belongs to an individual with asthma is

$$P(Asthma|X) = \frac{P(X|Asthma)P(Asthma)}{P(X)}$$

where $P(X|Asthma)$ is the likelihood of a microbiome sample (X) occurring given all the microbiome data from the asthmatic cohort, $P(Asthma)$ is the prior probability of any MARS patient having asthma, and $P(X)$ is the probability of the microbiome data (X) occurring given the entire MARS microbiome dataset (X). To accommodate the sparsity and zero-inflation inherent to microbiome data, we built our NBC to fit relative abundance data to a mixture distribution. We model $P(X|Asthma)$ and $P(X|Healthy)$ (see Figure 2A: pink and purple, respectively) as mixtures of (1) a beta distribution of relative abundance when the taxon is present and (2) a binary distribution when the taxon is not detected,

$$P(X|Class) = \begin{cases} P(Not\ Detected|Class) & x = 0 \\ (1 - (Not\ Detected|Class))Beta(X, \alpha, \beta|Class), & x \geq 0 \end{cases}.$$

By modeling the frequency of non-detection separately from relative abundance we increase the sensitivity of our model to learn differences in sparse taxa. The prior probability of a patient having asthma ($P(A)$) was determined based on the proportion of patients with asthma used in the training data. The beta distribution for each taxon was fit by Maximum a Posteriori estimation using Newton's Method, given a Gaussian prior. Hyperparameters of the prior distributions were optimized by a grid search. Using mixture distributions generated for each taxon in the model, we constructed a Naïve Bayes' Classifier in R to predict patient asthma status based on microbiome composition. The NBC produces metrics that are useful for further analysis, including a Feature Score which can be described as the log likelihood ratio of a taxon occurring at a given relative abundance in stool from an asthma donor compared to from a healthy donor. The Feature Score per taxon (i) per sample (j) is $F_{ij} = \log\left(\frac{P(X_i = x_{ij}|Asthma)}{P(X_i = x_{ij}|Healthy)}\right)$.

For each sample, the Feature Scores for all taxa (n) in a sample are summed to calculate the Sample Score, which can be described as the log likelihood of the sample being from the asthma population rather than the healthy. The Sample Score per sample is

$$S_j = \sum_i^n F_{ij}.$$

Samples were classified as asthmatic if the Sample Score was positive, and healthy if negative.

We identified taxa concordant with the model in any given healthy-asthma dyad by calculating the Pairwise Feature Score between the two samples for each ASV. The Pairwise Feature Score for a taxon in a dyad is then calculated as the difference between the Feature Score for the taxon in the sample with asthma and the Feature Score of the same taxon in the healthy control is

$$PFS_{ij_{AJ_H}} = F_{ij_{Asthmatic}} - F_{ij_{Healthy}}$$

ASVs in a dyad with a positive pairwise feature score were considered concordant with the model. See examples in Figure S2A.

Random forest

The random forest model (RF) was created in R using the randomForest package[97] (v4.6-14). All forests included 1000 trees (ntrees=1000) with 30x30 tree sampling with replacement (sampsize=c(30,30)) and were built on the same 392 ASVs used in the NBC.

Model evaluation

All AUC and ROC curve values were calculated in R using pROC (v1.16.2). ROC curve and AUC values in Figure 2C were calculated based on the sample scores for the NBC and tree classification votes for the RF. Platt-scaling was performed using the glm (family = binomial(logit)) and predict functions in R. We performed leave-one-out cross-validation (LOOCV) and repeated this process 100 times to estimate an average LOOCV classification rate. The NBC achieved a leave-one-out cross validation (LOOCV) accuracy of 75.8% (Figures S8C and S8D), which is similar to studies of comparable size,[25,98] and performed as well as a Random Forest classifier (LOOCV accuracy: 75.1%), another tool commonly used to classify disease-associated microbiome data. Taxa identified as highly discriminatory by the NBC were highly correlated with those found to be important by Random Forest (Figure S8A and Table S7, rho = 0.4439, p-value <0.0001, Spearman Correlation).